A Theory of Macromolecular Chemotaxis

Article *in* The Journal of Physical Chemistry B · May 2013

DOI: 10.1021/jp302587d · Source: PubMed

4 authors, including:

J. Michael Schurr
University of Washington Seattle
182 PUBLICATIONS **4,389** CITATIONS
SEE PROFILE

Bryant S Fujimoto
University of Washington Seattle
69 PUBLICATIONS **1,639** CITATIONS
SEE PROFILE

THE JOURNAL OF PHYSICAL CHEMISTRY B

Article

pubs.acs.org/JPCB

A Theory of Macromolecular Chemotaxis

J. Michael Schurr,* Bryant S. Fujimoto, Leticia Huynh, and Daniel T. Chiu

Department of Chemistry, University of Washington, Box 351700, Seattle, Washington 98195-1700, United States

Supporting Information

ABSTRACT: A macromolecule in a gradient of a cosolute that is preferentially (relative to the solvent) either attracted to or excluded from the domain of the macromolecule should experience a thermodynamic force and move, respectively, up or down the gradient. A theory of chemotactic forces arising from such preferential interactions, especially short-range ligand binding and excluded volume interactions, is developed via an extension of Kirkwood–Buff theory. The ligand binding result is confirmed for both non-ionic and ionic cosolutes by standard solution thermodynamics. The effect of increasing the electrolyte concentration to diminish the electrostatic free energy of a charged macromolecule is also treated formally via an electrostatic macromolecule–electrolyte preferential interaction coefficient. For short-range interactions, the induced chemotactic velocity is attributed entirely to tangential tractions at the interface between the macromolecule and its surrounding solution. The velocity of a spherical macromolecule driven by such tractions is derived by a hydrodynamic calculation for steady-state creepy flow with a partial slip boundary condition. Qualitative comparisons of theoretical predictions with experimental observations of Zheng and Pollack pertaining to charged microspheres near the surfaces of non-ionic gels suggest that the reported exclusion zones are due to chemotaxis induced by gradients of base (NaOH) (or acid (HCl)) and salt. With a single adjustable parameter, namely, the ratio of slip length to area per surface carboxyl (or amidine) group, this theory yields nearly quantitative agreement with many observations. The estimated slip length for the microspheres is comparable to that obtained for bovine serum albumen by fitting the chemotactic theory to two reported cross-diffusion coefficients. When a solution with a gradient of NaOH is placed in contact with a smooth glass wall, chemotactic surface tractions are predicted to cause convection of the solution toward the acidic end of the gradient, as observed in preliminary experiments.

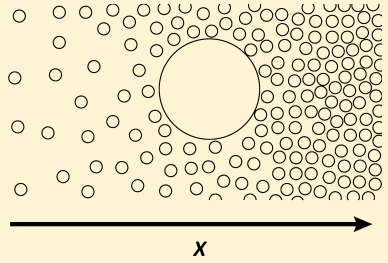

INTRODUCTION

Chemotaxis typically refers to the response of a motile biological organism to a concentration gradient of a particular solute. Net translation of the organism toward either higher or lower concentration of that solute exemplifies chemotaxis. Can non-living objects, including single molecules, also exhibit chemotaxis? It is intuitively expected that a molecule suspended in a liquid with a non-equilibrium gradient of any intensive thermodynamic variable will experience a non-vanishing thermodynamic force and move preferentially either up or down that gradient. Thus, it is expected that a molecule suspended at constant T and P in a chemical potential gradient of another solute species will experience a force and move one way or the other. The possibility of molecular chemotaxis was first suggested under the name of cross-diffusion in 1932,[1] and measurements of cross-diffusion were reported as early as 1955.[2,3] The history, experimental methods, selected experimental results, and previous theoretical developments pertaining to cross-diffusion were recently reviewed.[4] Numerous experiments have demonstrated unequivocally that a flux of one solute component can be induced by a gradient of another, which is the essence of cross-diffusion/molecular chemotaxis (cf. ref 4 and citations therein). Experiments to measure cross-diffusion coefficients (i.e., off-diagonal elements of the matrix of mutual translational diffusion coefficients of the various electroneutral solute components) have reached a fairly advanced stage, as demonstrated by the determination of all nine elements of the 3 × 3 mutual diffusion matrices of particular three-component solutes.[5,6] However, a satisfactory theory to predict a given off-diagonal matrix element (D_{ij}), which represents the induced flux or particle current density (concentration times mean velocity) of the ith electroneutral solute component per unit gradient of the concentration of the jth electroneutral component, is largely lacking except for dilute solutions of low-valent electrolytes[1,8−11] and solutions of alkanes of different sizes.[12] Especially for macromolecules, which have very large surface areas, either *net* exclusion or *net* binding of a cosolute *relative to the solvent* can significantly modulate the macromolecular chemical potential.[7] In that event, a gradient of such a solute will generate a chemotactic/cross-diffusion force on the macromolecule relative to the fluid in which it is suspended. Chemotaxis of a colloidal particle induced by a gradient of low molecular weight cosolute has also been called "diffusiophoresis",[13,14] and both theoretical and experimental investigations have appeared under that name.[15−20] Diffusiophoresis is tantamount to induced flow of a fluid adjacent to a solid surface (of the macromolecule), whenever the fluid contains a gradient of a solute that interacts preferentially (relative to solvent) with that surface.[20]

Received: March 17, 2012
Revised: May 2, 2013
Published: May 8, 2013

   dx.doi.org/10.1021/jp302587d | J. Phys. Chem. B 2013, 117, 7626–7652

Potential applications of molecular chemotaxis in microfluidics were recently demonstrated by the use of transverse salt gradients to either augment or oppose diffusive transport of negatively charged fluorescein from one flow stream to another,[21] or to narrow (focus) or spread (defocus) the lateral distribution of colloids in a longitudinally flowing stream by up to ∼50 μm over a flow distance of ∼0.84 mm.[22] In neither the cross-diffusion nor diffusiophoresis literature have chemotactic forces arising from interactions of ultrashort range, such as hard-core exclusion forces or, especially, chemical binding forces, been treated previously. Before reviewing previous cross-diffusion and diffusiophoresis theories and presenting the relevant new theory, it is important to describe certain topical phenomena, some of which are most likely previously unrecognized manifestations of macromolecular chemotaxis. These provide both motivation for the present study and experimental tests of the resulting theory.

Exclusion Zones and the Ordered Water Hypothesis. In a series of publications,[23−32] Pollack and co-workers reported numerous observations pertaining to the long-range effects of various surfaces on their surrounding solutions. Surfaces exhibiting long-range effects included various non-ionic and ionic hydrogels, ionomeric Nafion membranes, ion exchange gel beads, muscle tissues, and even a carboxylated monolayer of an alkyl thiol absorbed on gold, although its exclusion zone was less distinct and much slower to develop. However, other surfaces, such as (fiber optic) glass, stainless steel, copper, silver, and gold, showed no long-range effects. A common feature of the exclusion-zone-forming materials is their ability to absorb bases (or acids) from the solution either by simple diffusion in the case of neutral gels, by electrochemical diffusion and ion exchange in the case of ionic gels, or by simple titration in the case of carboxylated alkylthiols absorbed on gold. The main long-range effect was the formation of exclusion zones. When a suitable hydrophilic surface was placed in contact with a solution that initially contained a homogeneous distribution of positively or negatively charged microspheres with diameters in the range 0.45−4.0 μm, which were plainly visible at 20× magnification, it was found in most (but not all) cases that the microspheres migrated away from that surface with an initial speed of ∼1.0 to a few μm/s and slowed to an apparent standstill after all of the spheres were excluded from a zone of ∼50 to ∼600 μm, depending upon the surface and other conditions.[23−31] These exclusion zones were regarded as equilibrium phenomena and were attributed to the formation of an extensive (∼200 μm) zone of "structured water",[23] more precisely a "physically distinct and less mobile phase of water that can coexist indefinitely with the contiguous solute-containing phase".[24,30] This "long-range water ordering"[32] was suggested to involve partial alignment of water molecules to form a "liquid crystalline structure"[25] that was further suggested to be "initiated through hydrogen bonding with the nucleating surface".[24,25] From experiments with fluorescein-labeled bovine serum albumen (BSA), fluorescein itself, and 6-methoxy-*N*-(3-sulfopropyl) quinolinium dye, the ordered water phase was inferred to exclude impurities of all sizes, including BSA and dye molecules, as well as charged microspheres.[24,25]

In this paper, the experimental data, specifically the microscopic observations of Pollack and co-workers,[23−31] are accepted at face value. However, the interpretations proposed by the Pollack group, and certain inferences drawn therefrom, not only fail to account for significant data from their own lab but conflict with many other well-established observations from other laboratories. Relevant problems with the proposed interpretations of the exclusion zone in terms of long-range ordered water include the following.

(1) It was never conclusively established whether the exclusion zone is an equilibrium phenomenon or instead a long-lived non-equilibrium transient effect. The reported data typically do not extend more than 20 min after the initial contact between the hydrophilic surface and the solution. It was stated in the earliest paper[23] that exclusion zones could persist "up to a day" and "sometimes more than a week". However, it was reported in a later paper[22] that exclusion zones appeared (in the presence of 0.01 M imidazole buffer) around the acid (H^+) form of a cation exchange gel bead and around the basic (OH^-) form of an anion exchange gel bead but did *not* form around either kind of bead *after its exchange capacity was exhausted* (e.g., by exchange of cations such as imidazolium (ImH^+) for H^+ in the former bead or by exchange of anions such as Cl^- or HCO_3^- for OH^- in the latter). This observation suggests that exclusion zones around these beads are not actually equilibrium states but arise in part as a consequence of the process of ion exchange between the solution and the ionic gel, and are no longer observed after that process has reached equilibrium. In another paper,[26] it was reported that anion exchange beads (with positive intrinsic charges) in the absence of buffer became exhausted after ∼2 weeks (probably due to exchange of adventitious HCO_3^- in the solution for OH^- in the gel), which sets the time-scale for equilibration of ion exchange in the case of these rather small (∼600 μm diameter) ionic gels. For larger ionic gels, this process could take much longer. Thus, non-equilibrium conditions could easily prevail for "more than a week".

(2) The possibility that long-range chemical gradients, such as a pH gradient, might be responsible for the exclusion zone was considered and rejected for three reasons,[23] all of which now appear to be invalid. (i) It was stated that such a pH gradient (or gradient of $\ln c_{NaOH}$ or $\ln c_{HCl}$) would generate an internal electric field and electrostatic potential difference between the gel and solution, similar to a liquid junction potential, due to the different diffusion coefficients of the positive and negative ions. This much is true. However, it was then asserted that liquid junction potentials extend only over very small distances (presumably much less than ∼200 μm). This statement is simply incorrect for *unstirred* solutions, such as those studied by Pollack and co-workers. Indeed, the subsequent measurement of both long-range pH gradients[29,31] and electrochemical potentials[26,27,31] that decline over distances of ∼200 μm from the surfaces of ionic gels and ionomers could be taken as an indication that such liquid-junction potentials actually do extend over a distance of ∼200 μm. (ii) It was asserted that any such gradient would be expected to diminish with time, "yet the exclusion zone persisted easily for hours". However, if H^+ or OH^- ions are either released from or absorbed by the gel due to ongoing ion exchange, as occurs for charged gels and ionomers, then the temporal duration of the pH gradient may be considerably longer than "hours", as already noted. In any case, the time required for an already formed 200 μm exclusion zone to disappear in the absence of any exclusion or other forces is the time required for microspheres of radius R = 1.0 μm to diffuse to a root-mean-squared displacement, $d \sim 200$ μm, which is given by $t = d^2/2(kT/6\pi\eta R) = 93\,170$ s ≅ 25.9 h. Thus, if chemotactic forces suffice to build an exclusion zone at early times, then that could

dx.doi.org/10.1021/jp302587d | J. Phys. Chem. B 2013, 117, 7626−7652

persist for many hours regardless of how quickly the chemotactic forces decline. (iii) It was stated that the "local translation velocity would be expected to be proportional to the local pH gradient, but Figure 11 (of ref 23) shows that (the) velocity (at a given time after contact of the solution with the gel) could be independent of distance from the gel surface" or at least surprisingly insensitive to distance from that surface, even for an initial distance as great as 250 μm. This remark was intended to illuminate a presumed contradiction. However, as will be shown, the theoretical chemotactic trajectories of carboxylated microspheres in a gradient of $\ln c_{NaOH}$, which evolves via diffusion from an initial step function at $t = 0$, are remarkably similar to the corresponding experimental trajectories for various starting positions from 0 to 240 μm, and their net displacements at a given time are likewise surprisingly insensitive to their initial distances from the gel surface. Hence, there is no contradiction, and no reason to reject the possibility that molecular chemotaxis of the microspheres in a pH gradient is responsible for the formation of exclusion zones.

(3) The exclusion phenomenon depends strongly on the pH of the microsphere suspension. For carboxylated microspheres around non-ionic poly(vinyl alcohol) (PVA) gels, the size of the exclusion zone declines to zero, as the pH of the alkaline microsphere suspension is decreased to match the pH (5.7) of the gel.[23] This was attributed to the loss of microsphere charge.[23] However, the midpoint of the carboxylate microsphere titration curve is expected to lie between 5.5 and 6.0, so the carboxylated microspheres should still retain nearly half their charge at pH 5.7. When the same PVA gels interact with amidinated microspheres, the size of the exclusion zone also declines to zero, as the pH of the acidic microsphere suspension is increased to pH 5.7. The pK_d of free amidinium is ~12.4, so the amidinated microspheres should be effectively fully charged at all pH $\lesssim$ 10.0. Thus, the complete absence of exclusion at pH 5.7 cannot be attributed to any significant loss of charge of the amidinated spheres, and seems unlikely to be caused by the partial loss of charge of the carboxylated microspheres. However, it could be attributed to the absence of any pH gradient, when the pH's of the gel and solution match.

(4) The proposed exclusion of proteins from the surfaces of hydrophilic gels and biological tissues would prevent proteolytic enzymes, such as trypsin, pepsin, chymotrypsin, and collagenase, from attacking solid or gel supramolecular substrates, contrary to numerous observations. In fact, gelatin gel spheres are both permeable to, and readily hydrolyzed by, trypsin.[33,34] Likewise, the actions of lysozymes and cellulases on cell walls and of lipases on lipid membranes are obviously not prevented by exclusion of such enzymes from those surfaces. Similarly, infection of cells by viruses of various sizes and shapes is not prevented by exclusion of such species. In this light, exclusion appears to be considerably less than a universal phenomenon.

(5) If the proposed ordered structure of water in the exclusion zone is assumed to prevail inside the gel, as would be inferred from Pollack's nucleation idea, then it should exclude solutes and its viscosity should differ substantially from the bulk value. Concentrations and diffusion coefficients of many species, including NaCl, KCl, urea, glucose, sucrose, BSA, and hemoglobin, in 1.5% agar gels were measured subsequent to immersion of solute-free gels in aqueous solutions of each.[35] After applying corrections to account for the fraction of the total volume ($\phi < 1.0$) that is free to dissolve the solute, and for the obstructive effect of the gel (modeled as randomly oriented rods), the diffusion coefficients and equilibrium concentrations obtained were all within experimental error (~2%) of those in bulk. For the salts, urea, and sugars, the total correction amounted to only ~2.0−3.3%. These results indicate that nearly all of the water in the gel is accessible to such solutes and that any difference in diffusion coefficient, or implied viscosity, between the water accessible to solute in the gel and that in the pure liquid is $\lesssim$2% of the latter value. In regard to viscosity, solute-accessible water in the gel, which is very nearly all the water therein, is evidently practically indistinguishable from bulk water.

(6) Translational and rotational diffusion coefficients (D_T and D_R, respectively) of 41 different soluble proteins have been calculated to high accuracy from their reported crystal structures plus a "solvation" layer of uniform thickness, 1.1 Å, which is considerably less than that of a water monolayer (~3.0 Å).[36] Agreement of the results with reported experimental values is well within the experimental errors in every case. Clearly, the outward extent of any ordered water at protein surfaces must be rather slight. Also, dynamic light scattering measurements of D_T for both lipid vesicles and charged polystyrene latex spheres yield hydrodynamic radii in the range ~10−200 nm that are in good agreement with the corresponding radii measured by electron microscopy and total intensity light scattering (unpublished results in the lab of J. M. Schurr). There is no indication of any ordered boundary water extending far into the surrounding solution.

In view of the aforementioned problems with the long-range ordered water hypothesis, an investigation of alternative explanations for the observed exclusion zones is warranted. In this study, we examine theoretically the possible role of macromolecular chemotaxis in the phenomena of exclusion or attraction of microspheres by *non-ionic* (neutral) hydrophilic gels. The more complex exclusion/attraction phenomena exhibited by ionic (charged) hydrophilic gels, which exhibit strong Donnan effects and undergo (counter) ion exchange, are analyzed in terms of long-range pH and/or salt gradients in a subsequent paper (II, 10.1021/jp302589y).[37] The reported long-range "electric" potentials are likewise ascribed to long-range pH and salt gradients in paper II (10.1021/jp302589y). Other properties, including spontaneous infrared emission images, and NMR T_2 images and pulsed-gradient spin−echo water-diffusion experiments, are also analyzed in paper II (10.1021/jp302589y), where problems concerning the interpretations of those experimental data in terms of ordered water are noted, and alternative interpretations that do not involve ordered water are proposed in each case.

Theories of Mutual Diffusion in Multicomponent Systems. Conventionally, cross-diffusion theory has focused on the flux, or current density, of the ith electroneutral component arising from the concentration gradient of the jth electroneutral component, which is denoted by $j_i = -D_{ij}\nabla c_j$. In this study, we are interested primarily in the mean drift velocity of the ith electroneutral component, which in cross-diffusion theory would be given by $u_i = (j_i/c_i) = -(D_{ij}/c_i)\nabla c_j$. This relation connects the chemotactic velocity to a relevant cross-diffusion coefficient. Of course, the simultaneous gradients of any other electroneutral components contribute in an additive fashion to the total j_i and $u_i = j_i/c_i$.

Previous conventional and dynamic light scattering mutual diffusion theories for multicomponent electrolyte solutions are reviewed in section S1 of the Supporting Information. Such theories, which do not account fully for either the distributions

of small ions or the perturbed fluid flow around the individual ions, work well for dilute univalent ions but become quantitatively increasingly erroneous with increasing macroion charge and size.

In cross-diffusion studies of highly charged bovine serum albumin (BSA) (component 3) in a 0.2 M two-component phosphate (pH 2.2) or two-component citrate (pH 4.5) buffer, the predicted D_{31} and D_{32} of the electroneutral component matrix were found to exceed the measured values by an order of magnitude for the citrate buffer and by several-fold with also an incorrect sign of D_{32} for the phosphate buffer.[38] Such large errors suggest that either the direct (non-hydrodynamic) forces on the polyions or their mobilities are much smaller than predicted by the standard cross-diffusion theories.

A theoretical prescription to compute elements of the mutual diffusion coefficient matrix for dilute spherical ionic species is given by eq 90 of ref 39 in the $q \rightarrow 0$ limit after projecting out the charged mode. This projection can be accomplished in a manner analogous to that used for eq 94 of that same article. Evaluation of these matrix elements requires as essential input all radial distribution functions and two-body hydrodynamic interaction tensors for spherical species of possibly very different charge and size. Calculation of the radial distribution functions of dilute solutions of highly charged polyions and their counterions and co-ions remains a challenging problem. Moreover, this theory applies only to circumstances wherein the direct (non-hydrodynamic) forces between spherical particles are center to center (normal to the surface) and have sufficiently great range. In theory, the zero velocity of approach at contact condition (from lubrication theory with stick boundary conditions)[40−45] greatly reduces the effects of short-range direct interactions and, in the case of mutual diffusion of hard spheres with hydrodynamic interactions, completely removes all effects of direct intersphere interactions on the mutual translational diffusion coefficient, except for backflow corrections.[40] Certain chemotactic forces exerted on a spherical macromolecule, such as those arising from cosolute exclusion or the binding of small cosolutes, have extremely short range, and a gradient of such a cosolute gives rise in a statistical sense to tangential (as well as normal) equal but oppositely directed forces on the macromolecular surface and its adjacent solution. The theory in ref 39 does not apply to such forces, which are treated by an entirely different approach in this study.

The effects of different partial molecular volumes in otherwise ideal solutions on cross-diffusion have been treated with some success.[12] While the different molecular volumes of solutes and solvents were taken into account in an approximate way, no account was taken of the exclusion of a cosolute relative to solvent at the surface of a solute molecule.[7] Cosolute exclusion can significantly increase the standard state chemical potential of a macromolecule,[7] so a gradient of excluded osmolyte can generate a significant force, as will be seen.

Theories of Diffusiophoresis. Theories of diffusiophoresis of spherical macromolecules in gradients of both nonelectrolytes and electrolytes have been developed.[15−18,20] The diffusiophoretic theory for electrolytes is briefly reviewed and critiqued in section S2 of the Supporting Information. Due to the stick boundary condition used, the range of the macromolecule−cosolute interaction must significantly exceed the thickness of the first water layer above the colloid surface in order to predict a non-vanishing velocity. Consequently, these theories do not apply to short-range excluded-volume or cosolute-binding interactions, which are treated here by an alternative route using a partial slip boundary condition. Diffusiophoretic theories for electrolyte gradients are not based upon thermodynamic arguments but instead upon the standard electrokinetic equations of electrophoresis theory, at least one of which is not entirely correct, as noted in section S2 of the Supporting Information. More significantly, no account is taken of the effect of electrolyte on the ionization equilibrium and the effect of that upon the macromolecular chemical potential and its gradient. The diffusiophoretic theories apply only to smooth spherical surfaces and predict velocities that depend only upon the electrostatic potential at that presumed surface of shear. However, the surfaces of real macromolecules and colloids are typically quite rough with much of the surface lying inside the surface of shear. Those charged groups inside the surface of shear still interact with salt, which may significantly lower the electrostatic free energy of the macromolecule, and contribute significantly to its chemical potential gradient, when it resides in a gradient of salt concentration. Such contributions to the driving force are entirely absent in the diffusiophoretic theories. In addition, the use of a pure stick boundary condition may be inappropriate in light of recent results indicating a small but finite slip on glass surfaces. Because of their different boundary conditions at the solid−fluid interface, the diffusiophoretic theory and the present theory are not readily compared.

In general, the diffusiophoretic theory yields two contributions: (1) a chemiphoretic theory that is presumably an approximate electrokinetic theory analogue of the present electrolyte theory after removing the contribution of electrolyte to alter the ionization constant of the acid (or base) groups on a macromolecule and (2) the electrophoretic contribution that arises from the internal electric field that accompanies the diffusion of neutral salt, when the cations and anions have different friction factors. Although an obvious choice for a motive force at first glance, no such contribution is considered here for reasons discussed in section S2 of the Supporting Information, which suggest that the internal electric field acting upon the macroion and its ion atmosphere may be significantly less than that associated with the neutral salt gradient.

Detailed Plan of the Paper. Extended Kirkwood−Buff (KB) theory is introduced and related to the thermodynamics of dilute macromolecular solutions that contain a cosolute.[7,46−53] The slope of the *standard state* chemical potential of the macromolecule with respect to the chemical potential of the cosolute is expressed in terms of KB integrals. This slope is evaluated in terms of (i) hard-core exclusion of the cosolute relative to water and (ii) cosolute−solvent exchange at sites on or near the macromolecular surface. The thermodynamic force is expressed in terms of this slope, which is just the negative of the *non-electrostatic* macromolecule−cosolute preferential interaction coefficient. The simple result for cosolute binding is confirmed by conventional solution thermodynamics for a nonionic cosolute in section S3 of the Supporting Information, and for an ionized electroneutral cosolute, NaOH, in Appendix B. The effect of electrolyte on the binding constant and electrostatic free energy of the macromolecule is expressed in terms of an *electrostatic* macromolecule−electrolyte preferential interaction coefficient. Thermodynamic forces arising from base or acid and salt gradients are expressed simply in terms of relevant parameters. The chemotactic velocity is calculated by solving the linearized Navier−Stokes equation for an incompressible viscous fluid subject to balanced surface

dx.doi.org/10.1021/jp302587d | J. Phys. Chem. B 2013, 117, 7626−7652

tractions (forces per unit area) and a partial slip boundary condition. The trajectories of carboxylated microspheres in a temporally evolving gradient of rather dilute base, typical of that in the experiments of Pollack and co-workers, are reckoned and compared with the experimental observations. A detailed comparison between predictions of the chemotactic theory and various results from the Pollack lab shows that molecular chemotaxis accounts qualitatively for practically all of the reported observations pertaining to microsphere interactions with non-ionic gels. With a single adjusted parameter, namely, the ratio of the slip length to the area per carboxyl group, this chemotactic theory accounts nearly quantitatively for many of those same observations. With a plausible area per carboxyl group, the estimated slip length of a microsphere resembles that obtained for BSA (component 3) by fitting the chemotactic theory to reported values of D_{31} and D_{32} in a two-component pH 2.2 phosphate buffer. The circumstance wherein a solution bearing a gradient of NaOH contacts a fixed surface, such as a glass wall, which bears acidic silanol groups that bind (or have bound) OH^- ions, is also analyzed, and gradient-induced convection of the liquid is predicted. Preliminary experiments are briefly discussed. Finally, possible roles and uses of molecular chemotaxis are noted.

THEORY

Results from K−B Theory. We consider solutions containing a negligibly small volume fraction of macromolecules (component 2) plus a dilute small-molecule cosolute (component 3) in a solvent (component 1), which is generally water in this study. The cosolute may be preferentially either accumulated at or excluded from the macromolecular surface. All independent components are electroneutral, and initially are taken to be non-ionic. Ionic components will be discussed subsequently. Eventually, we shall treat the situation wherein there is a non-equilibrium gradient of the concentration of 3, but first we discuss relevant thermodynamic properties of two- and three-component solutions at equilibrium. We use several results from the theory originated by Kirkwood and Buff[46] and extended by Ben-Naim, Smith, and others.[7,47−53]

Thermodynamic Considerations. We shall usually treat the limit of infinitely dilute macromolecules, $c_2 \to 0$. In this case, the solution surrounding a macromolecule is effectively a two-component solution of 1 and 3. For such a solution, the variation of the chemical potential of 3 (μ_3 J/molecule) with increasing concentration of 3 (c_3 molecules/m^3) at constant T and P is given by

$$(1/kT)(\partial\mu_3/\partial \ln c_3)_{T,P} = 1/(1 + c_3(G_{33} - G_{31})) \quad (1)$$

where $G_{ij} = \int_V d^3\mathbf{r}(g_{ij}(r) - 1) = G_{ji}$ is a Kirkwood−Buff integral over a suitably large volume V and $g_{ij}(r) = g_{ji}(r)$ is a pair correlation function for the species i and j, as a function of the distance (r) between the (arbitrarily chosen) central atoms of i and j, and $d^3\mathbf{r} = dx\, dy\, dz$ is a volume element. Equation 1 can be obtained directly for a two-component solution[46,49,53] and also by treating a three-component system at constant T, P, and c_2 and taking the limit $c_2 \to 0$ (cf. eqs 42 and 45 of ref 53). Although $g_{ij}(r)$ depends upon the choice of central atom, G_{ij} does not. The derivation of eq 1 via grand ensemble fluctuation theory applies to any choice of central atoms of the molecules involved.[7] The G_{ij} all approach finite limiting values as c_3 approaches zero. When c_3 is sufficiently small that c_3 $(G_{33} - G_{31})$ is negligible compared to 1.0, then $(\partial\mu_3/\partial \ln c_3)_{T,P} = kT$. This relation is integrated over $d \ln c_3$ at constant T and P to obtain the well-known *dilute* solution result

$$\mu_3 = \mu_3^0 + kT \ln c_3 \quad (2)$$

where μ_3^0 is that part of the chemical potential that is independent of c_3, and is called the standard state chemical potential. μ_3^0 applies to a fictitious state wherein $c_3 = 1.0$ molecules/m^3, but the environment of each 3-molecule is that of an infinitely dilute solution $c_3 \to 0$, which corresponds to pure solvent in this case.

For a three-component solution of 1, 2, and 3, the variation of the chemical potential of 2 (μ_2) with increasing molality of 2 (m_2) at constant molality of 3 (m_3) is given by

$$(1/kT)(\partial\mu_2/\partial \ln m_2)_{T,P,m_3} = 1/(1 + c_2\cdot\Delta) \quad (3)$$

where

$$\Delta \equiv G_{22} + G_{13} - G_{12} - G_{23} + A_1A_3/(c_1A_3 + c_3A_1) \quad (4a)$$

$$A_1 = 1 + c_1(G_{11} + G_{23} - G_{12} - G_{13}) \quad (4b)$$

$$A_3 = 1 + c_3(G_{33} + G_{12} - G_{13} - G_{23}) \quad (4c)$$

Equation 3 is obtained from the last of eqs 28 of ref 53 after interchanging the 3 and 2 indices, and eqs 4a−4c follow from eqs 5 and 29 of that same paper. The quantities c_1 and c_3, the KB integrals in eqs 4a−4c, and hence Δ all approach finite limiting values, as c_2 becomes small at constant m_3. Hence, $c_2\cdot\Delta$ becomes negligibly small compared to 1.0 in the limit of sufficiently small c_2. In that limit, eq 3 can be rewritten as

$$(\partial\mu_2/\partial \ln m_2)_{T,P,m_3} = kT \quad (5)$$

Integrating eq 5 over $d \ln m_2$ at constant T, P, and m_3 yields the *dilute* solution result

$$\mu_2 = \tilde{\mu}_2^0 + kT \ln m_2 \quad (6)$$

where $\tilde{\mu}_2^0$ pertains to a 1.0 m standard state, wherein each 2-molecule experiences the environment of an infinitely dilute (in regard to component 2) solution, which consists of 1 and 3 with molality m_3. The molality, m_2, can be expressed in terms of c_2 (molecules/m^3) by $m_2 = c_2(55.6)\bar{V}_1/(N_A\phi_1) \simeq c_2/((1000)N_A\phi_1)$ mol/kg, where $\phi_1 = 1 - (c_2\bar{v}_2 + c_3\bar{v}_3) = 1 - \phi_2 - \phi_3$ is the thermodynamic volume fraction of solvent, N_A is Avogadro's number, $\bar{v}_2$ and $\bar{v}_3$ are the partial molecular volumes of 2 and 3, respectively, and $\bar{V}_1 = N_A\bar{v}_1 \cong 1.8 \times 10^{-5}$ m^3 mol^{-1} is the partial molar volume of 1 (i.e., water). Equation 6 can be rewritten as

$$\mu_2 = \mu_2^0 + kT \ln c_2 \quad (7)$$

where $\mu_2^0 = \tilde{\mu}_2^0 - kT\ln[(1000)N_A\phi_1]$ and pertains to the fictitious 1.0 molecules/m^3 standard state, wherein each 2-molecule has the environment of a solution that is infinitely dilute in 2 ($c_2 \to 0$) but with the same m_3 and $m_1 = 55.6$ (mol/kg) of the remaining solution. Again, μ_2^0 is that part of the macromolecular chemical potential that is independent of c_2. However, μ_2^0 generally depends upon the composition of the two-component solution of 1 and 3 that constitutes the environment of each 2-molecule in its standard state. At constant T and P, a two-component solution has only a single independent chemical potential, which is here taken to be μ_3. The variation of μ_2^0 with μ_3 at constant T, P, and c_2^∞ is given by

$$\Gamma_3(2) \equiv -(\partial\mu_2^0/\partial\mu_3)_{T,P,c_2^\infty} = c_3(G_{32} - G_{12}) \quad (8)$$

dx.doi.org/10.1021/jp302587d | J. Phys. Chem. B 2013, 117, 7626−7652

where c_2^∞ denotes $c_2 \to 0$.[7,50,53] The symbol $\Gamma_3(2)$ denotes a (non-electrostatic) preferential interaction coefficient (PIC).[7] It has been shown via Kirkwood–Buff theory that

$$\Gamma_3(2) = (\partial m_3/\partial m_2)_{T,\mu_1,\mu_3} \tag{9}$$

for any value of c_2, including c_2^∞ (cf. eqs 13 and 47 of ref 53). Equations 8 and 9 in principle apply to any electroneutral component 3, whether non-ionic or ionic, but the right-hand side (rhs) of eq 8 is useful only in situations where $g_{32}(r)$ is well-defined. This requires that an electrolyte ion, such as a co-ion of the macroion, that uniquely represents the local electrolyte concentration, must exist, which is always the case in a three-component system, when all intrinisic charges on the macroion have the same sign. Equation 9 provides a measure of the net binding of cosolute 3 to, or the net exclusion of 3 from, the domain of macromolecule 2. A positive value of $\Gamma_3(2)$ is sometimes described as thermodynamic binding of cosolute, and a negative value of $\Gamma_3(2)$ is typically characterized as cosolute (or osmolyte) exclusion.

Evaluation of $\Gamma_3(2)$ in Terms of Molecular Properties. A heuristic evaluation of the $\Gamma_3(2)$ for a non-ionic cosolute 3 was given in terms of a hard-core excluded-volume contribution plus a contribution from cosolute–water exchange reactions at sites accessible to the non-ionic cosolute near the macromolecular surface.[7] The excluded volume contribution is simply

$$\Gamma_3^{ex}(2) = -c_3\Delta V^{ac} \tag{10}$$

where $\Delta V^{ac} = V_3^{ex} - V_1^{ex}$ is the difference between the volume excluded to cosolute centers and that excluded to water centers by a macromolecule and is normally positive. The increase in μ_2^0 due to this excluded volume effect, when the cosolute concentration is raised from 0 to c_3, is just $\Delta\mu_2^0 = (\partial\mu_2^0/\partial\mu_3)_{T,P,c_2^\infty}(\partial\mu_3/\partial c_3)_{T,P}(c_3 - 0) = c_3\Delta V^{ac}(kT/c_3)c_3 = kTc_3\Delta V^{ac} = \Pi\Delta V^{ac}$.

This is just the reversible work to expel the centers of cosolute molecules at osmotic pressure, $\Pi \equiv c_3kT$, from the volume ΔV^{ac}. For any cosolute that is larger than water, this work is positive, and acts to increase μ_2^0 above its value in pure water. When a macromolecule is added to a binary solution of water plus cosolute, its hard-core excluded volume forces exert two effects: (1) the volume of the solution is increased by the macromolecular volume, $\bar{v}_2$, that is excluded to any part of a water or cosolute molecule; (2) cosolute centers are excluded from a region that is still accessible to water centers but which was also accessible to cosolute centers before addition of the macromolecule. The increase in chemical potential of the macromolecule is associated with the latter demixing (osmotic exclusion) effect. This simple interpretation is only valid when the larger (more excluded) species 3 is dilute, in the sense that its volume fraction is rather small.

The exchange reaction contribution is evaluated as follows. We assume that each macromolecule (P) has $M \gg 1$ identical independent sites, at each of which the exchange reaction

$$P{\cdot}(H_2O)_\nu + L \rightleftharpoons P{\cdot}L + \nu H_2O \tag{11}$$

can occur. The quantity, $P{\cdot}(H_2O)_\nu$, denotes a single site containing $\nu \cong \bar{v}_3/\bar{v}_1$ water molecules, L denotes a free cosolute (ligand) molecule, and P·L denotes the same site occupied by a cosolute molecule. The equilibrium constant for an exchange reaction at this site is

$$K = \frac{[P{\cdot}L](a_1)^\nu}{[P{\cdot}(H_2O)_\nu]a_3} \tag{12}$$

where a_1 is the activity of water and a_3 is that of the cosolute. The fraction of sites occupied by the cosolute is

$$f = \frac{[P{\cdot}L]}{[P{\cdot}(H_2O)_\nu] + [P{\cdot}L]} = \frac{Ka_3(a_1)^{-\nu}}{1 + Ka_3(a_1)^{-\nu}} \cong \frac{Kc_3}{1 + Kc_3} \tag{13}$$

The last expression in eq 13 is obtained by invoking the assumption that the cosolute is sufficiently dilute that $a_3 \cong c_3$ and $a_1 \cong 1.0$. This assumption prevails throughout the remainder of this paper. It is shown in Appendix A that the exchange reaction contribution is

$$\Gamma_3^{er}(2) = M(Kc_3 - (c_3/c_1)\nu)/(1 + Kc_3) \tag{14}$$

Whenever $K > \nu/c_1 \cong \bar{v}_3/\phi_1 \simeq \bar{v}_3$, which holds for all binding sites of significance when $\phi_1 \approx 1.0$, $\Gamma_3^{er}(2)$ is positive and causes a decrease in μ_2^0 with increasing c_3.

Summing the excluded volume and exchange reaction contributions yields the total non-electrostatic PIC

$$\begin{aligned}\Gamma_3(2) &= \Gamma_3^{ex}(2) + \Gamma_3^{er}(2)\\ &= -c_3\Delta V^{ac} + M(Kc_3 - (c_3/c_1)\nu)/(1 + Kc_3)\end{aligned} \tag{15}$$

When the exchange constants K and M are sufficiently large, the binding sites are nearly saturated at such a low $c_3 \approx 10/K$ that $c_3\Delta V^{ac} \ll M$, and the $MKc_3/(1 + Kc_3) \simeq M$ term predominates. In this case, $\Gamma_3(2)$ is positive and μ_2^0 decreases with increasing c_3. In this same limit, wherein the cosolute binding term predominates, the variation of μ_2^0 with c_3 is given by

$$\begin{aligned}(\partial\mu_2^0/\partial c_3)_{T,P,c_2^\infty} &= -\Gamma_3(2)(\partial\mu_3/\partial c_3)_{T,P,c_2^\infty}\\ &= -MkTK/(1 + Kc_3)\end{aligned} \tag{16}$$

where eq 2 has been employed. Equation 16 shows explicitly how μ_2^0 declines with increasing c_3. This variation of the free energy per macromolecule with increasing concentration of a binding cosolute can also be obtained directly from ordinary solution thermodynamics, without recourse to Kirkwood–Buff theory, as shown in detail in section S3 of the Supporting Information. The total free energy of the solution decreases as the initially empty binding sites of the macromolecule spontaneously equilibrate with the prevailing chemical potential of species 3. This decrease in free energy per macromolecule is the contribution of the binding reaction to μ_2^0, and $(\partial\mu_2^0/\partial c_3)_{T,P,c_2^\infty \to 0}$ is just the variation of that contribution with c_3. An advantage of the Kirkwood–Buff formulation is that it encompasses the case of weak as well as strong binding, and also the case where excluded volume interactions make an important or even dominant contribution to $\Gamma_3(2)$, whereas ordinary solution thermodynamics does not.

Thermodynamic Forces Arising from Chemical Potential Gradients. We now consider a solution at constant T and P, wherein small non-equilibrium gradients of c_2 and c_3 (and c_1) prevail. All macroscopic gradients are assumed to lie in the x-direction. The chemotactic force in the x-direction exerted on the rather dilute 2 macromolecules is taken to be

dx.doi.org/10.1021/jp302587d | J. Phys. Chem. B 2013, 117, 7626–7652

$$F_{ch}(x) = -(d\mu_2/dx)_{T,P}$$
$$= -(\partial\mu_2^0/\partial\mu_3)_{T,P,c_2^\infty}(\partial\mu_3/\partial c_3)_{T,P,c_2^\infty}dc_3/dx - (\partial(kT\ln c_2)/\partial c_2)_{T,P}dc_2/dx$$
$$= +\Gamma_3(2)(kT/c_3)(dc_3/dx) - (kT/c_2)dc_2/dx \quad (17)$$

The last term, which arises from the gradient of c_2, is the thermodynamic force that drives ordinary mutual diffusion of any dilute species. (A $(1 - \phi_2)^{-1}$ correction must be applied, when ϕ_2 is not negligibly small.[39,54]) Diffusion is a reasonably well understood process that need not be considered further in this study, except insofar as it predicts the evolution of cosolute gradients in time. In contrast, the first term arises from the gradient of μ_2^0 due to the gradient of any dilute cosolute that exhibits significant positive or negative preferential interactions (relative to solvent) with the macromolecule.

When $\Gamma_3(2)$ is negative, as is the case when excluded volume interactions predominate, the cosolute gradient force in eq 17 is in the opposite direction to the cosolute gradient. In other words, the macromolecule moves toward a region with a lower cosolute concentration in order to lower its chemical potential. Conversely, when $\Gamma_3(2)$ is positive, as is the case when the macromolecule exerts a strong binding affinity for cosolute (relative to solvent), the cosolute gradient force in eq 17 is in the same direction as the cosolute gradient. In this case, the macromolecule lowers its chemical potential by moving toward a region of higher cosolute concentration, as illustrated schematically in Figure 1.

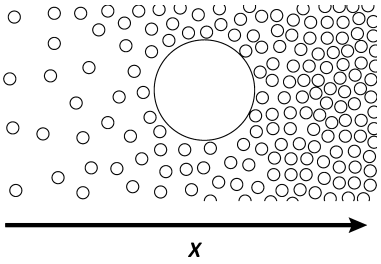

Figure 1. Schematic illustration of a spherical macromolecule in a concentration gradient of much smaller cosolute molecules. If the cosolute accumulates preferentially (relative to solvent) in the vicinity of the macromolecule, the latter experiences a force in the $+x$ direction. Conversely, if the cosolute is excluded preferentially (relative to solvent) from the vicinity of the macromolecule, the latter experiences a force in the $-x$ direction.

The Excluded Volume Force. The chemotactic force arising from the different volumes excluded by the macromolecule to cosolute and solvent centers is given simply by $F_{ch} = -(V_3^{ex} - V_1^{ex})kT\,dc_3/dx$ and is directly proportional to the concentration gradient. Consider a spherical macromolecule of radius $R = 1\ \mu m = 10^{-4}$ cm suspended in a 0.1 M solution of glycerol in water. The effective radius of glycerol is $R_3 = (1/2)(\bar{v}_3)^{1/3} = 2.45 \times 10^{-8}$ cm, and that of water is $R_1 = (1/2)(\bar{v}_1)^{1/3} = 1.48 \times 10^{-8}$ cm. The volume excluded to glycerol centers is $V_3^{ex} = (4\pi/3)(R + R)^3$, and that excluded to water centers is $V_1^{ex} = (4\pi/3)(R + R_1)^3$, which gives $V_3^{ex} - V_1^{ex} = 1.219 \times 10^{-15}$ cm^3. If the glycerol gradient is $dc_3/dx = 6.022 \times 10^{19}$ molecules/cm^4, which corresponds to 0.1 M cm^{-1}, the predicted force at 293 K is $F_{ch} = -2.97 \times 10^{-9}$ dyn $\cong$ −0.030 pN. Larger forces would require a larger spherical macromolecule, a larger cosolute, or a greater cosolute gradient.

The Force Arising from Cosolute Binding. Upon substituting eq 16 (valid when $K \gg \bar{v}_3$) into the first term of eq 17, we obtain the chemotactic force arising from neutral cosolute binding

$$F_{ch} = MkT(K/(1 + Kc_3))(dc_3/dx)_{T,P,c_2^\infty}$$
$$= MkT(Kc_3/(1 + Kc_3))(d\ln c_3/dx)_{T,P,c_2^\infty} \quad (18)$$

which predominates whenever $MK/(1 + Kc_3) \gg \Delta V^{ac}$. F_{ch} has the same sign as $(dc_3/dx)_{T,P,c_2^\infty}$, so the macromolecules in this case should move toward a higher concentration of c_3.

Under near saturation conditions, when $Kc_3 \gg 1.0$, this force is given simply by

$$F_{ch} = MkT(d\ln c_3/dx)_{T,P,c_2^\infty} \quad (19)$$

Because this force is proportional to the gradient of $\ln c_3(x)$ rather than simply the gradient of $c_3(x)$, it depends only upon the relative shape of the concentration profile, $c_3(x)/c_3(x_0)$, where x_0 is an arbitrary position in the gradient, but not upon its magnitude, $c_3(x_0)$. Thus, two cosolute concentration profiles with the same relative shape, $c_3(x)/c_3(x_0)$, but differing in magnitude, $c_3(x_0)$, by a factor of 10 or 100 or more, would generate the same force on the macromolecule, provided that the conditions $Kc_3 \gg 1.0$ and $c_3\Delta V^{ac} \ll M$ hold for both profiles. Thus, c_3 can be neither too small nor too large in order to observe this invariance of the force to the magnitude of $c_3(x_0)$.

When c_3 is sufficiently small that $Kc_3 \ll 1.0$, then

$$F_{ch} = MkTKc_3(d\ln c_3/dx)_{T,P,c_2^\infty} = MkTK(dc_3/dx)_{T,P,c_2^\infty} \quad (20)$$

Thus, for a fixed value of $(\partial \ln c_3/dx)_{T,P,c_2^\infty}$, F_{ch} vanishes in the limit $Kc_3 \to 0$. In this limit, the exchange (or binding) sites for 3 are all unoccupied. For a given relative concentration profile of cosolute, the force is maximal when all exchange (or binding) sites are fully occupied by cosolute, and is zero when they are completely empty.

We note that $d\ln c_3 = (1/c_3)dc_3$ is unitless, as is the product Kc_3. Hence, in eqs 18−20, any concentration unit can be employed for c_3, provided K has the corresponding inverse unit, without altering the value of the calculated force.

Consider a spherical macromolecule of radius $R = 1\ \mu m = 10^{-4}$ cm bearing $M = 10^5$ surface binding sites with $K = 10^8$ M^{-1} =1.66 × 10^{-19} m^3/molecule. The area per binding site is $A_{ch} = 1.26 \times 10^4$ Å^2. The ligand concentration is assumed to be $c_3 = 10^{-6}$ M, so $c_3K = 100$ and $f \cong 0.99$. The ligand gradient is assumed to be $dc_3/dx = 0.1$ M cm^{-1}, as assumed for the excluded volume force. The predicted force on the sphere at 293 K is $F_{ch} = 4.00 \times 10^{-4}$ dyn = 4000 pN. This force exceeds by 1.33×10^5-fold that reckoned above for excluded volume interactions in the case of glycerol with a similar gradient. If the ligand has the same volume as glycerol, the inequality, $MK/(1 + Kc_3) \gg \Delta V^{ac}$, is well satisfied for all c_3 from 0 to 0.0136 M.

Choice of Components. For the purpose of evaluating either $\Gamma_3(2)$ or the chemotactic force, F_{ch}, the macromolecular component 2 must be regarded as the bare species, whose environment, including waters of hydration and bound cosolute molecules, contributes to its chemical potential. It is essential that *all* exchangeable water and cosolute species, whether bound or free, must appear in $g_{32}(r)$, $g_{12}(r)$, G_{32}, and G_{12}.

dx.doi.org/10.1021/jp302587d | J. Phys. Chem. B 2013, 117, 7626−7652

Binding of Electoneutral Ionic Bases to Acid Groups of Macromolecules. The above theory applies to the binding of electroneutral ionic cosolute bases, specifically $Na^+ + OH^-$, to electroneutral ionic or non-ionic macromolecular species. We verify this assertion in the following way. We consider a macromolecule (P) bearing M identical electroneutral acid groups, which could be carboxylic acid, sulfuric acid, sulfonic acid, phosphoric acid, or silanol groups. We focus here on carboxylic acid (−COOH) groups. In a thermodynamic sense, each carboxylic acid group is capable of binding an electroneutral $Na^+ + OH^-$ "molecule" according to

$$P{-}COOH + Na^+ + OH^- \rightleftharpoons P{-}COO^- + Na^+ + H_2O \tag{21}$$

After the reaction, the Na^+ ion, or another one that could be substituted for it, is electrostatically confined to the domain of the macromolecule, just as it was confined to the domain of the OH^- beforehand. In addition, a molecule of H_2O is released from the macromolecule. Hence, eq 21 can be regarded as an exchange reaction, wherein one "molecule" of ionized NaOH is thermodynamically bound to, and a H_2O is released from, the same site on the macromolecule.

In this case, the cosolute NaOH comprises two dilute ions, Na^+ and OH^-, each of which contributes as an effectively independent particle to lower the solvent chemical potential. Of course, when the charge density of a macromolecule is so large that it becomes a strong polyelectrolyte, the electrostatic free energy per negative charge is much greater for the polyanion than for OH^- ions, and this has significant consequences, as will be seen in the next section. For simplicity, we first conduct a thermodynamic analysis of spontaneous NaOH binding in Appendix B, wherein the small ions are regarded simply as independent particles, and no account is taken of the electrostatic free energy of the macromolecule. The results in eqs B7 and B8 are identical to those for a non-ionic cosolute in eqs 16 and 18, provided that, in the latter, $K = K_b$, where $K_b = (c_{PCOO^-})(X_1)/(c_{PCOOH})(c_{OH^-})$ is the equilibrium constant for reaction 21, $c_{OH^-} = c_{NaOH}$ is the concentration of OH^- ions, and $X_1 \simeq 1.0$ is the mole fraction of solvent (H_2O). In this sense, eqs 16 and 18 are verified for macromolecules of sufficiently low charge density that the electrostatic free energy of a carboxylate group, $-COO^-$, is comparable to that of a hydroxide ion, OH^-, in which case the electrostatic free energy affects both reactants and products similarly and exerts no significant influence on the binding reaction 21. In this case, the chemotactic OH^--binding force exerted on the macromolecule by a gradient of OH^- ligands is

$$F_b = MkT(K_b c_{OH^-}/(1 + K_b c_{OH^-}))(\mathrm{d} \ln c_{OH^-}/\mathrm{d}x)_{T,P,c_P^\infty} \tag{22}$$

which is identical to eq 18, if species 3 is NaOH.

Electrostatic Free Energy and the Effects of Monovalent Electrolyte. The electrostatic free energy (ΔG_P^{el}) of a macromolecule of fixed size with charges all of the same sign is generally positive, and increases with increasing number of charges but decreases with increasing concentration of monovalent electrolyte, S. The electrolyte S could be either monovalent salt or monovalent ionic base (or acid), and in general is the sum of both, so $c_S \equiv c_{salt} + c_{OH^-}$ (or $c_S = c_{salt} + c_{H^+}$). Such electrolyte may increase K_b in eq 22 and also decrease the electrostatic free energy of the polyion and provides an additional *electrolyte gradient* force.

A. Effect of Electrolyte on the Equilibrium Constant for OH^- Binding. The effect of electrolyte on the equilibrium constant for an arbitrary reaction involving one or more electroneutral polyanion components, $P \equiv P(COO^-)_N{\cdot}(Na^+)_N$, $N \le M$, each of which dissociates completely to its polyanion, $A^{N^-} \equiv P(COO^-)_N$, and its $NX^+ \equiv Na^+$ counterions, is given by[55]

$$(\partial \ln K_b/\partial \ln c_S)_{T,P,c_P^\infty} = -2H + 2\Delta\Gamma_S \tag{23}$$

Here, H is the net number of "molecules" of neutral small-ion salt produced by the reaction and $\Delta\Gamma_S$ is the difference in *electrostatic* PIC of the neutral polyanion species for the small-ion electrolyte between products on one hand and reactants on the other. For the reaction in eq 21, we can set $H = 0$ and treat OH^- as a polyanion of unit charge. Also, during the reaction $P(COO^-)_N \rightarrow P(COO^-)_{N+1}$, as one more carboxyl group is titrated, and the counterion of the consumed OH^- becomes a counterion of the new polyanion component, $P(COO^-)_{N+1}{\cdot}(Na^+)_{N+1}$, which is also completely dissociated. Thus, $\Delta\Gamma_S \equiv \Gamma_S(P(COO^-)_{N+1}) - \Gamma_S(P(COO^-)_N) - \Gamma_S(OH^-) \cong 1{\cdot}\partial\Gamma_S(P(COO^-)_N)/\partial N - \Gamma_S(OH^-)$.

In general, for a completely dissociated polyanion component, $A^{N^-} + NX^+$, immersed in a solution of monovalent electrolyte, $S = X + Y$, where $X \equiv X^+$ and $Y \equiv Y^-$ are monovalent cation and anion, respectively, at concentration $c_X = c_S = c_Y$, the electrostatic PIC for electrolyte is given by[56,57]

$$\Gamma_S(A^{N^-}) = \int \mathrm{d}^3\mathbf{r}(c_Y(\mathbf{r}) - c_Y) \tag{24}$$

The integral is taken over the entire volume of a solution containing a single polyanion, and is clearly the net number of excess co-ions in the ion atmosphere of the polyanion. Because co-ions are always excluded to some extent, $\Gamma_S(A^{N^-})$ is always negative. The neutral electrolyte concentration at position $\mathbf{r}$ in the ion atmosphere of A^{N^-} is precisely equal to the co-ion concentration, $c_Y(\mathbf{r})$, at that same point, so $\Gamma_S(A^{N^-})$ pertains equally to net excess electrolyte in the ion atmosphere of $A^{N^-} \equiv P(COO^-)_N$. It is known that $\Gamma_S(P(COO^-)_N) \cong -N/2$ whenever $\kappa\delta \gg 1.0$, where δ is the spacing between nearest-neighbor charges and κ is the Debye screening parameter, which is given by $\kappa = (3.28 \times 10^7)I^{1/2}$ (cm^{-1}), where I is the ionic strength. In this limit, each $-COO^-$ group behaves like an isolated monovalent anion, for which linear Poisson−Boltzmann (LPB) theory approximately applies, and the number of excess co-ions per intrinsic charge is $\Gamma_{1S}(P(COO^-)) \equiv (1/N)\Gamma_S(P(COO^-)_N) = \Gamma_S(OH^-) \cong -1/2$. However, $(1/N)\Gamma_S(P(COO^-)_N)$ increases (becomes less negative) with increasing N, whenever non-linear Poisson−Boltzmann (NLPB) theory applies. In this case, the compensating charge in the ion atmosphere comes more from an excess of (positive) counterions and less from a deficit of (negative) co-ions. Thus, in general, $-N/2 \le \Gamma_S(P(COO^-)_N) < 0$, which implies that $-1/2 \le \partial\Gamma_S(P(COO^-)_N)/\partial N < 0$. Consequently, $\Delta\Gamma_S$ must lie in the range $0 \le \Delta\Gamma_S < 1/2$.

B. Effect of Electrolyte on the Chemical Potential of the Macromolecule. The standard state chemical potential of the macromolecule bearing M carboxyl groups is given by

$$\mu_P^0(c_{OH^-}^0, c_{salt}^0) = \mu_{P(COOH)}^0 + (\partial\Delta G/\partial n_P^0)_{T,P,n_w^0,n_{NaOH}^0} + \Delta G_P^{el} \tag{25}$$

dx.doi.org/10.1021/jp302587d | J. Phys. Chem. B 2013, 117, 7626−7652

where $\mu^0_{P(COOH)}$ pertains to the non-ionic $P(COOH)_M$ species, the second term on the right-hand side arises from OH^- binding and is given by eq B6, and the third term is the electrostatic free energy of the resulting polyanion, $P(COO^-)_N$, bearing $N = fM$ intrinsic (carboxylate) charges, where $f \equiv (K_b c_{OH^-}/(1 + K_b c_{OH^-}))$ is the fraction of titrated (ionized) carboxyl groups. It is noteworthy that the OH^--binding reaction 21 does not change the number of Na^+ ions in the solution, so $\mu^0_{P(COOH)}(c^0_{OH^-}, c^0_{salt})$ contains no $N\mu_{Na^+}$ term due to either net binding or net release of counterions, and represents the free energy change upon adding a single non-ionized macromolecule to the solution in which it subsequently ionizes. Differentiating eq 25 with respect to $d \ln c_S$ at constant T, P, and c_P^∞ and constant c_{OH^-} in the $K_b c_{OH^-}$ terms yields

$$\begin{aligned}
&(\partial \mu_P^0/\partial \ln c_S)_{T,P,c_P^\infty,\hat{c}_{OH^-}} \\
&= -kTM\left(\frac{\partial \ln(1 + K_b c_{OH^-})}{\partial \ln K_b}\right)_{T,P,c_P^\infty,\hat{c}_{OH^-}} \\
&\quad \left(\frac{d \ln K_b}{d \ln c_S}\right)_{T,P,c_P^\infty,\hat{c}_{OH^-}} + \left(\frac{d\Delta G_P^{el}}{d \ln c_S}\right)_{T,P,c_P^\infty,\hat{c}_{OH^-}} \\
&= -kTMf\{2\partial\Gamma_S(P(COO^-)_N)/\partial N - 2\Gamma_S(OH^-)\} \\
&\quad - kTMf\{1 + 2\Gamma_{1S}(P(COO^-)_N)\} \\
&= -kTMfW
\end{aligned} \tag{26}$$

where the relation $(\partial \Delta G_P^{el}/\partial \ln c_S)_{T,P,c_P^\infty} = -kT(N + 2\Gamma_S(P(COO^-)_N))$[55−58] was employed, f is given just above, and

$$W \equiv 2\{1 + \partial\Gamma_S(P(COO^-)_N)/\partial N + \Gamma_{1S}(P(COO^-)_N)\} \tag{27}$$

The $\hat{c}_{OH^-}$ subscripts in eq 26 indicate that the value of c_{OH^-} in the $K_b c_{OH^-}$ terms remains constant, when $c_S = c_{salt} + c_{OH^-}$ is varied (in the sense of differentiation) by varying c_{OH^-}. Using the ranges $-1/2 \le \partial\Gamma_S(P(COO^-)_N)/\partial N < 0$ and $-1/2 \le \Gamma_{1S}(P(COO^-)_N) < 0$, we find that $0 \le W \le 2.0$. Thus, $(\partial \mu_P^0/\partial \ln c_S)_{T,P,c_P^\infty,\hat{c}_{OH^-}}$ is always either vanishing or negative. This is expected, since there is always either a vanishing or positive net excess of small ions (counterions plus co-ions) in the ion atmosphere of any polyion, which can be regarded as a vanishing or net positive preferential *electrostatic* interaction with constituents of the surrounding electrolyte solution, despite the exclusion of co-ions.

The slope of μ_P^0 with respect to $\ln c_{OH^-}$ due solely to OH^- binding at constant (possibly vanishing) salt concentration is obtained from eq 22 as

$$(\partial \mu_P^0/\partial \ln c_{OH^-})^{bind}_{T,P,c_P^\infty,c_{salt}} = -kTMf \tag{28}$$

The total slope of μ_P^0 with respect to c_{OH^-} is the sum of that in eq 28 plus that in eq 26 multiplied by $\partial \ln c_S/\partial \ln c_{OH^-} = c_{OH^-}/(c_{salt} + c_{OH^-})$, namely,

$$\begin{aligned}
&(\partial \mu_P^0/\partial \ln c_{OH^-})^{tot}_{T,P,c_P^\infty,c_{salt}} \\
&= -kTMf\{1 + (c_{OH^-}/(c_{salt} + c_{OH^-}))W\}
\end{aligned} \tag{29}$$

In general, the factor in curly braces lies in the range $1.0 \le 1 + W < 3.0$.

The total slope of μ_P^0 with respect to $\ln c_{salt}$ is that in eq 26 multiplied by $\partial \ln c_S/\partial \ln c_{salt} = c_{OH^-}/(c_{salt} + c_{OH^-})$, namely,

$$(\partial \mu_P^0/\partial \ln c_{salt})_{T,P,c_2^\infty,c_{OH^-}} = -kTMf(c_{salt}/(c_{salt} + c_{OH^-}))W \tag{30}$$

In the limit $c_{salt} \gg c_{OH^-}$, eq 30 becomes precisely eq 26 with $c_S = c_{salt}$, as expected. In the limit $c_{OH^-} \gg c_{salt}$, $(\partial \mu_P^0/\partial \ln c_{salt})_{T,P,c_2^\infty,c_{OH^-}}$ becomes negligibly small compared to $(\partial \mu_P^0/\partial \ln c_{OH^-})^{tot}_{T,P,c_2^\infty c_{salt}}$, whenever $\partial \ln c_{OH^-}/\partial x$ and $\partial \ln c_{salt}/\partial x$ are roughly comparable.

Total Forces on Negatively Charged Microspheres Arising from Gradients of OH^- and Salt. The total force arising from a gradient of OH^- in the presence of an arbitrary concentration of salt is obtained from eq 29 as

$$\begin{aligned}
F_{OH^-} &\equiv -(\partial \mu_P^0/\partial \ln c_{OH^-})_{T,P,c_P^\infty,c_{salt}}(d \ln c_{OH^-}/dx)_{T,P,c_P^\infty,c_{salt}} \\
&= kTMf\{1 + (c_{OH^-}/(c_{salt} + c_{OH^-}))W\} \\
&\quad (d \ln c_{OH^-}/dx)_{T,P,c_P^\infty,c_{salt}}
\end{aligned} \tag{31}$$

where $f = K_b c_{OH^-}/(1 + K_b c_{OH^-})$ and W is given by eq 27. The second term is generally positive and acts to augment the first term, so F_{OH^-} is always directed along the hydroxide gradient. The second term is negligible compared to the first whenever $c_{salt} \gg c_{OH^-}$, or when $W \sim 0$.

The total force arising from a salt gradient in the presence of an arbitrary concentration of OH^- is obtained from eq 29 as

$$\begin{aligned}
F_{salt} &= -(\partial \mu_P^0/\partial \ln c_{salt})_{T,P,c_P^\infty,c_{OH^-}}(d \ln c_{salt}/dx)_{T,P,c_P^\infty,c_{OH^-}} \\
&= +kTMf(c_S/(c_{salt} + c_{OH^-})W(d \ln c_{salt}/dx))
\end{aligned} \tag{32}$$

In both eqs 31 and 32, W should be evaluated for $N = fM$. F_{salt} is always directed along the salt gradient.

At times, it will be useful to consider the total electrolyte gradient force, $F_S = kTMfW(d \ln c_S/dx)_{T,P,c_P^\infty,\hat{c}_{OH^-}}$, which is the sum of the second term in F_{OH^-} plus F_{salt}. The total chemotactic force can then be written as

$$\begin{aligned}
F_{ch} &= kTMf\{(\partial \ln c_{OH^-}/dx)_{T,P,c_P^\infty,c_{salt}} \\
&\quad + W(\partial \ln c_S/dx)_{T,P,c_P^\infty,\hat{c}_{OH^-}}\}
\end{aligned} \tag{33}$$

The subscript $\hat{c}_{OH^-}$ on $(d \ln c_S/dx)_{T,P,c_P^\infty,\hat{c}_{OH^-}}$ means that the c_{OH^-} concentration in the $K_b c_{OH^-}$ terms is held constant, while c_{OH^-} in $c_S = c_{OH^-} + c_{salt}$ is varied.

Analysis of *W*. Some insight into the maximum value of W (cf. eq 27), and the conditions under which its minimum ($W = 0$) and maximum ($W = 2.0$) values prevail, is gained as follows. Whenever linear Poisson−Boltzmann (LPB) theory is valid, one has $\Gamma_S(P(COO^-)_N) = -N/2$, $\partial\Gamma_S(P(COO^-)_N)/\partial N = -1/2$, $\Gamma_{1S}(P(COO^-)_N)/\partial N = -1/2 = \Gamma_S(OH^-)$,[56,57] and $W = 0$.

Approximate values of $\Gamma_{1S}(P(COO^-)_N)$ can be estimated for a spherical particle whenever the surface of the sphere is smooth and uniformly charged and the ion atmosphere thickness is thin compared to the particle radius, so $\kappa R \ge 30$. For such an effectively flat uniformly charged surface, an analytical expression for $\Gamma_{1S}(P(COO^-)_N)$ has been derived[57] from the analytical (Gouy−Chapman) solution of the NLPB equation, as described in section S4 of the Supporting Information. The relevant expression (eq S4.6, Supporting Information) is

dx.doi.org/10.1021/jp302587d | J. Phys. Chem. B 2013, 117, 7626−7652

$$\Gamma_{1S}(P(COO^-)_N) = -A_{ch}2c_S(1/\kappa)(1 - 1/(\sigma_d + \sqrt{\sigma_d^2 + 1})) \quad (34)$$

where A_{ch} is the average surface area per intrinsic charge and $\sigma_d = (1/A_{ch})e_0^2 2\pi/(\varepsilon kT\kappa)$ is the dimensionless surface charge density. When $A_{ch} \to \infty$, then $\sigma_d \to 0$, and $\Gamma_{1S}(P(COO^-)_N) \to -1/2$, as expected. When $A_{ch} \to 0$, then $\sigma_d \to \infty$, and $\Gamma_{1S}(P(COO^-)_N) \to 0$, as expected.

If $R = 10^{-4}$ cm, $\varepsilon = 80$, $T = 293$ K, $e_0 = 4.8 \times 10^{-10}$ esu (protonic charge), and C_S is the molar electrolyte concentration, then $\kappa = 3.28 \times 10^7\ C_S^{1/2}$ cm^{-1}, and $c_S = C_S N_{Av}/1000$ molecules/cm^3, where $N_{Av} = 6.022 \times 10^{23}$ is Avogadro's number. The condition $\kappa R \geq 30$ is obeyed for all $C_S \geq 10^{-4}$ M, and even when $C_S = 10^{-5}$ M, $\kappa R = 10.4$, so the thin ion atmosphere condition almost holds there as well. If we assume that $\partial\Gamma_S(P(COO^-)_N)/\partial N = \Gamma_{1S}(P(COO^-)_N)$, then it is also possible to estimate W. If $A_{ch} = 10^{-12}$ cm^2/charge (10^4 Å^2/charge), then the estimated values of $\Gamma_{1S}(P(COO^-)_N)$ and W range from $\Gamma_{1S}(P(COO^-)_N) = -0.103$ and $W = 1.6$ at $C_S = 10^{-5}$ M to $\Gamma_{1S}(P(COO^-)_N) = -0.466$ and $W = 0.14$ at $C_S = 10^{-2}$ M. However, if $A_{ch} = 10^{-14}$ cm^2/charge (100 Å^2/charge), the values of $\Gamma_{1S}(P(COO^-)_N)$ and W range from $\Gamma_{1S}(P(COO^-)_N) = -0.001$ and $W = 2.0$ at $C_S = 10^{-5}$ M to $\Gamma_{1S} = -0.035$ and $W = 1.9$ at $C_S = 0.01$ M. Typically, $A_{ch} \leq 100$ Å^2/charge for microspheres, so it is likely that W takes a value not far from 2.0 over the range of electrolyte concentrations considered here. In that case, the electrolyte (second) term in eq 31 exceeds by nearly 2.0-fold the pure binding (first) term in that same equation, whenever $c_{OH^-} \gg c_{salt}$. However, the surfaces of the microspheres are locally quite rough, and the distribution of intrinsic charges is most likely rather heterogeneous with A_{ch} possibly being so small in some regions as to limit ionization, while being much greater in others. In such a case, Γ_{1S} could well be significantly lower (more negative) than zero, and the corresponding value of W could be significantly smaller than these values estimated for smooth uniformly charged surfaces with $A_{ch} = 100$ Å^2/charge. For the same value of A_{ch}, the F_{salt} term in the chemotactic force

$$F_{ch} = F_{OH^-} + F_{salt} \quad (35)$$

would be expected to exceed F_{OH^-}, whenever $c_{salt} > 3c_{OH^-}$ and $(d\ln c_{salt}/dx)_{T,P,c_P^\infty,\hat{c}_{OH-}} > (d\ln c_{OH-}/dx)_{T,P,c_P^\infty,c_{salt}}$.

The foregoing analysis of W was based upon the assumption that $\partial\Gamma_S(P(COO^-)_N)/\partial N \simeq \Gamma_{1S}(P(COO^-)_N)$. Given the observation that $\Gamma_{1S}(P(COO^-)_N)$ increases with increasing N, it is readily shown that $\partial\Gamma_S(P(COO^-)_N)/\partial N \geq \Gamma_{1S}(P(COO^-)_N)$. Consequently, when $\Gamma_{1S}(P(COO^-)_N)$ is close to zero (only slightly negative), $\partial\Gamma_S(P(COO^-)_N)/\partial N$ is even closer to zero (less negative). Hence, the preceding estimates of this derivative and W are lower bounds.

Effect of Electroneutral Ionic Acids on Macromolecules Bearing Acid Groups. Macromolecules bearing acid groups spontaneously dissociate in water, but in the presence of an acid, such as $H^+ + Cl^-$, the extent of this dissociation is diminished. The free energy change upon equilibrating the dissociation reaction

$$PCOOH \rightleftharpoons PCOO^- + H^+ \quad (36)$$

is evaluated in section S5 of the Supporting Information, and used to obtain the force F_{ba} in the presence of an HCl gradient, which is given in eq S5.8 (Supporting Information). This force is in the direction of lower H^+, or higher OH^-, concentration. Equation S5.8 (Supporting Information) may be rewritten in the following way. Combining reaction 36 with the reverse of eq 21 yields the net reaction

$$H_2O \rightleftharpoons H^+ + OH^- \quad (37)$$

with equilibrium constant $K_w = 10^{-14} = K_d/K_b$, where $K_d = 1/K_a$ is the acid dissociation constant. Hence, the acid association constant is $K_a = 1/K_wK_b$. By using this relation together with $c_{H^+} = K_w/c_{OH^-}$ in eq S5.8 (Supporting Information), we obtain precisely eq 22. Thus, F_{ba} and F_b are one and the same, as might have been anticipated. It is important to note that the force falls off and becomes very small when $K_ac_{H^+} \gg 1$ or, equivalently, when $K_bc_{OH^-} \ll 1.0$, and the macromolecule is practically untitrated (non-ionized).

Binding of Electroneutral Ionic Acids to Basic Groups on Macromolecules. We consider a macromolecule P bearing M identical electroneutral basic groups, which could be amine, amidine, or guanidine groups. Here we focus on primary amine ($-NH_2$) groups. Each amine group can thermodynamically bind an electroneutral $H^+ + Cl^-$ "molecule" according to

$$P{-}NH_2 + H^+ + Cl^- \rightleftharpoons P{-}NH_3^+ + Cl^- \quad (38)$$

After the reaction, the Cl^- ion, or one substituted for that, is electrostatically confined to the domain of the macromolecule, just as it was confined to the domain of the H^+ beforehand. In this case, the analysis and results are identical to those obtained for base binding to acid groups with the following replacements: $c_{OH^-} \to c_{H^+}$, $K_b \to K_a = (c_{PNH_3^+})/(c_{PNH_2})(c_{H^+})$, $\Gamma_{1S}(PCOO^-) \to \Gamma_{1S}(PNH_3^+)$, and $\Gamma_{1S}(OH^-) \to \Gamma_{1S}(H^+)$. Moreover, for a cation, A^{N^+}, with N intrinsic positive charges, immersed in a solution of monovalent electrolyte, $S = X + Y$ ($X \equiv X^+$, $Y \equiv Y^-$) at concentration $c_X = c_S = c_Y$, the PIC for electrolyte per intrinsic polyion charge is

$$\Gamma_{1S}(A^{N+}) = (1/N)\int d^3\mathbf{r}(c_X(\mathbf{r}) - c_X) \quad (39)$$

Thus, eqs 22, 23, 25, 26, 32, and 35 become, respectively, eqs 40–45 below.

$$F_a = MkTf(d\ln c_{H^+}/dx)_{T,P,c_P^\infty} \quad (40)$$

where $f = K_ac_{H^+}/(1 + K_ac_{H^+})$ is the protonated fraction of amine groups.

$$(\partial\ln K_a/\partial\ln c_S)_{T,P,c_2^\infty} = -2H + 2\Delta\Gamma_S \quad (41)$$

where $\Delta\Gamma_S \equiv 1(\partial\Gamma_S(P(NH_3^+)_N)/\partial N) - \Gamma_S(H^+)$, and $H = 0$ for reaction 38.

$$\mu_P^0(c_{H^+}, c_{salt}) = \mu_{Pn}^0 + (\partial\Delta G/\partial n_P^0)_{T,P,n_w^0,n_{HCl}^0} + \Delta G_P^{el} \quad (42)$$

where μ_{Pn}^0 pertains to the neutral $P(NH_2)_M$ species. The total proton gradient force is

$$F_{H^+} = kTMf\{1 + (c_{H^+}/(c_{salt} + c_{H^+}))W\}(d\ln c_{H^+}/dx)_{T,P,c_P^\infty,c_{salt}} \quad (43)$$

where $W = 2\{1 + \partial\Gamma_S(P(NH_3^+)_N)/\partial N + \Gamma_{1S}(P(NH_3^+)_N)\}$. The total force arising from a salt gradient is

$$F_{salt} = kTMf\cdot(c_{salt}/(c_{salt} + c_{H^+}))W(d\ln c_{salt}/dx)_{T,P,c_P^\infty,c_{H^+}} \quad (44)$$

dx.doi.org/10.1021/jp302587d | J. Phys. Chem. B 2013, 117, 7626–7652

In eqs 43 and 44, W is to be evaluated for $N = fM$. The total chemotactic force contains the contributions of both proton and salt gradients

$$F_{ch} = F_{H^+} + F_{salt} \tag{45}$$

A Simple Interpretation of the Ligand Binding Force. In the limit, $f \rightarrow 1.0$, where practically all of the $-COOH$ groups have bound an NaOH to become a $-COO^-$ group plus its counterion, a particularly simple picture of the driving force for translation of the macromolecule emerges. Translation of the polyion without comigration of its counterions is effected by first converting it to the neutral $P(COOH)_M$ species by carrying out the reverse of eq 21 for each $-COO^-$ group, which injects M OH^- ions into the solution at that position (x_1) but does not affect the number of Na^+ ions there. After translating the now neutral $P(COOH)_M$ species to another place in the gradient (x_2), the polyanion is recharged to the same extent according to eq 21 by absorbing M OH^- ions from the solution at that point (x_2), but that does not affect the number of Na^+ ions there either. Thus, the migration process involves no net translocation of Na^+ ions from one point to another but does involve the removal of M OH^- ions from the solution (and attachment of those to a $P(COOH)_M$) at x_2 and the injection of M OH^- ions (from the reaction $P(COO^-)_M + M\ H_2O \rightarrow P(COOH)_M + M\ OH^-$) into the solution at x_1. This is tantamount to translocation of M OH^- from x_2 to x_1 in concert with translocation of $P(COO^-)_M$ from x_1 to x_2.

The negative of the resulting change in free energy per unit translation of the $P(COO^-)_M$ due to the OH^- dissociation and rebinding steps in this case is given by

$$-\Delta G_{tr}/(x_2 - x_1) \equiv MkT(\ln[c_{OH^-}(x_2)] - \ln[c_{OH^-}(x_1)])/(x_2 - x_1) \tag{46}$$

Equation 46 is just a discretized version of eq B8 in the (assumed) limit $f = 1.0$. Thus, for a completely titrated polyanion, the combined OH^- dissociation and rebinding steps give the primary contribution to the OH^--binding force in an NaOH gradient. The total OH^- gradient force, given in eq 31 contains also a correction term, $(c_{OH^-}/(c_{salt} + c_{OH^-}))W$, in the curly braces that takes into account the electrolyte contribution to decrease the electrostatic free energy of the charged macromolecule directly and also indirectly by increasing the binding constant for the OH^- binding reaction.

Induced Velocity. A chemotactic force, F_{ch}, acting on a macromolecule is manifested by an induced velocity

$$u = F_{ch}/\zeta \tag{47}$$

where ζ is the relevant friction factor. For a spherical macromolecule that is propelled by an external agent through a liquid with stick boundary conditions, ζ is given by Stokes law

$$\zeta = 6\pi\eta R \tag{48}$$

where R is the macromolecular radius and η is the viscosity of the solution containing components 1 and 3. However, when a pair of spherical molecules in solution interact via an intermediate- or long-range potential that gives rise to opposing center-to-center direct forces on the two spheres, hydrodynamic interactions act to diminish, but not reverse, the sphere velocities induced by those forces.[40] Such hydrodynamic interactions increase in magnitude with decreasing distance between the spheres and, according to lubrication theory with stick boundary conditions, reduce the velocities of both spheres to zero at the contact distance.[41−45] Thus, under contact or near contact conditions, Stokes law is totally inadequate.

Surface Tractions and the Hydrodynamic Calculation. We now consider the circumstance wherein small spheres in solution interact with the surface of a very much larger sphere by such short-range forces that significant strength of interaction occurs only at or very near the contact distance, where no solvent molecules intervene between the two surfaces. Under such conditions, the normal component of the force is unable to induce significant relative motion of the two spheres along their line of centers, because at or near contact hard-core repulsions prevent their moving significantly closer together, and the force vanishes when the spheres move far enough apart to admit the first layer of intervening water molecules. Moreover, for all forces whose range is very small compared to the radius of the large sphere, hydrodynamic interactions nearly cancel the direct center-to-center forces. When such contact or very short-range interactions predominate, they give rise (in a statistical sense) to a free energy per unit area of the interface between the large sphere and the solution containing the small spheres, which could be either excluded osmolytes or ligands that bind to surface sites on the larger sphere. When there exists a gradient of small sphere concentration in the solution with a component tangent to the large sphere surface, there will be a gradient of the surface free energy per unit area, which in turn gives rise to a tangential force per unit area, or traction, at the large sphere−solution interface. This tangential traction acts with equal strength, but in opposite directions, on the large sphere and the solution containing the small spheres. The ligand binding and excluded volume contributions to the chemotactic force, F_{ch}, are true contact forces, whereas the range of the electrostatic interactions is the Debye length, $1/\kappa$. The latter force is treated only approximately by regarding it as a contact interaction in F_{ch}, as is done here. Any contact forces normal to the surface of the large sphere involve only those small spheres and solvent molecules at the contact distance, and are not transmitted to the other small spheres or solvent molecules in the solution. Consequently, no pressure gradient is expected in the surrounding solution, and any motion of the large sphere relative to the solution must arise entirely from the tangential tractions. Hence, $\nabla P = 0$, and there are no body forces to consider, so the steady-state linear (creepy flow) Navier−Stokes equation becomes

$$\nabla^2\mathbf{v} = 0 \tag{49}$$

where $\mathbf{v}$ is defined as the fluid velocity in a coordinate frame attached to a stationary microsphere.

Of course, no tangential motion of the fluid relative to the sphere can arise from contact tractions unless the stick boundary condition is replaced by something like the partial slip condition, as described below. The fluid is practically incompressible, so $\nabla\cdot\mathbf{v} = 0$. In this example, $\nabla \times (\nabla \times \mathbf{v}) = \nabla(\nabla\cdot\mathbf{v}) - \nabla^2\mathbf{v} = 0$, which can be satisfied by $\nabla \times \mathbf{v} = 0$. This condition in turn can be satisfied by $\mathbf{v} = \nabla\phi$, where ϕ is a scalar. By taking $\nabla^2\phi = 0$, the conditions $\nabla\cdot\mathbf{v} = 0$ and $\nabla^2\mathbf{v} = 0$ are both satisfied (the latter because the operators ∇^2 and ∇ commute). This reasoning suggests that ϕ is a sum of well-known solutions of Laplace's equation with coefficients to be determined by the boundary conditions.

Consider the diagram in Figure 2. The origin of the coordinate system is taken at the center of a stationary microsphere of radius R, which is suspended in a fluid

dx.doi.org/10.1021/jp302587d | J. Phys. Chem. B 2013, 117, 7626−7652

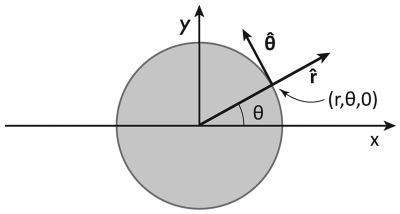

Figure 2. Coordinates for the hydrodynamic calculation. The shaded area is a planar section passing through the center of the spherical macromolecule. The +x-axis is parallel to the relevant thermodynamic force on the sphere, and is chosen as the polar axis of a polar coordinate system. The y-axis is chosen to lie in the planar section, and the z-axis (not shown) points toward the viewer. The unit vectors, $\hat{\mathbf{r}}$ and $\hat{\boldsymbol{\theta}}$, in the planar section are indicated.

(solution) that moves with velocity $\mathbf{v} = -u\hat{\mathbf{x}}$, at large distances from the sphere, where $\hat{\mathbf{x}}$ is a unit vector along the +x axis. Gradients of ln c_{OH^-} and/or ln c_{salt} lie along +$\hat{\mathbf{x}}$, which is taken to be the polar axis for spherical polar coordinates. We consider an infinitesimal patch of microsphere surface with area $\delta A = R^2 \sin\theta\, d\phi\, d\theta$. The y-axis and unit vector, $\hat{\mathbf{y}}$, are chosen so that this patch intersects the xy plane, which coincides with the plane of the figure, and the z-axis is perpendicular to the xy plane, extending outward toward the viewer. The patch has Euclidean coordinates (x, y, 0) and spherical polar coordinates (R, θ, 0). The unit vectors, $\hat{\mathbf{r}} = \hat{\mathbf{x}}\cos\theta + \hat{\mathbf{y}}\sin\theta$, and $\hat{\boldsymbol{\theta}} = \hat{\mathbf{x}}\sin\theta + \hat{\mathbf{y}}\cos\theta$, in the xy plane are also indicated.

As noted above, the component of a chemotactic contact force along a normal to the patch (i.e., along $\hat{\mathbf{r}}$) produces no significant motion of the sphere relative to its adjacent fluid. However, the tangential component of that force per unit area is a traction that simultaneously pushes the patch in the $-\hat{\boldsymbol{\theta}}$ direction (toward greater x) and the solution in the $+\hat{\boldsymbol{\theta}}$ direction (toward smaller x). The chemotactic force exerted on the patch by the solution can be written as

$$\mathbf{F}_{ch}^{pat} = kT\sigma(\delta A) f G \hat{\mathbf{x}} \tag{50}$$

where

$$G = \{(\partial \ln c_{OH^-}/\partial x)_{T,P,c_p^\infty,c_{salt}} + W(\partial \ln c_S/\partial x)_{T,P,c_p^\infty,\hat{c}_{OH^-}}\} \tag{51}$$

is the gradient factor and σ is the number of surface acid groups per unit area. The chemotactic force exerted on the solution by the patch is, $\mathbf{F}_{ch}^{sol} = -\mathbf{F}_{ch}^{pat}$. The tangential component of the chemotactic force *per unit area* exerted on the solution by the patch is $(\mathbf{F}_{ch}^{sol}\cdot\hat{\boldsymbol{\theta}}/\delta A)\hat{\boldsymbol{\theta}} = (kT\sigma f G \sin\theta)\hat{\boldsymbol{\theta}}$. In addition, the patch exerts a viscous traction on the fluid at the interface, $\mathbf{T}_{vis}^{sol} = -\eta(\partial v_\theta(R,\theta)/\partial r)\hat{\boldsymbol{\theta}}$. In the steady state, the total force per unit area exerted by the patch on the fluid surface must vanish, so $(\mathbf{F}_{ch}^{sol}\cdot\hat{\boldsymbol{\theta}}/\delta A)\hat{\boldsymbol{\theta}} + \mathbf{T}_{vis}^{sol} = 0$, which yields

$$\eta\partial v_\theta(R,\theta)/\partial r = kT\sigma f G \sin\theta \tag{52}$$

The equivalent result for a flat surface is derived by a more elaborate argument in Appendix E.

The boundary conditions for the fluid velocity are

$$v_r(R,\theta) = 0 \tag{53a}$$

$$v_\theta(R,\theta) = \lambda\partial v_\theta(R,\theta)/\partial r \tag{53b}$$

$$\lim(r\to\infty)v_x = v_r(r,\theta)\cos\theta - v_\theta(r,\theta)\sin\theta = -u \tag{53c}$$

where u is the microsphere velocity in the +$\hat{\mathbf{x}}$ direction relative to stationary fluid at large distance. According to eq 53c, the x-component of the fluid velocity in the frame of the stationary sphere is then $-u$ at large distance. Equation 53b is known as the partial slip condition, and λ is the slip length. Combining eqs 52 and 53b yields

$$v_\theta(R,\theta) = (kT\sigma f G\lambda/\eta)\sin\theta \tag{54}$$

which gives the tangential fluid velocity (in the reference frame of the microsphere) at the microsphere surface in terms of parameters governing the chemotactic force, the slip length, λ, and the solution viscosity, η. Note that $v_\theta(R,\theta)$ is positive for all values of θ in its allowed range, $0 \le \theta \le \pi$, so its x-component is always negative, as expected. This property holds for all values of $r \ge R$, as will be seen.

The scalar (flow) potential, ϕ, is taken to be the $l = 1$ solution of Laplace's equation

$$\phi = aP_1(\cos\theta)/r^2 + brP_1(\cos\theta) = a\cos\theta/r^2 + br\cos\theta \tag{55}$$

where $P_1(\cos\theta)$ denotes the rank 1 Legendre polynomial. This yields

$$v_r = \partial\phi/\partial r = -2a\cos\theta/r^3 + b\cos\theta \tag{56a}$$

$$v_\theta = (1/r)\partial\phi/\partial\theta = -a\sin\theta/r^3 - b\sin\theta \tag{56b}$$

where a and b are coefficients to be determined by the boundary conditions. Applying eq 53a (eq 54) to eq 56a (eq 56b) yields

$$-2a/R^3 + b = 0 \tag{57a}$$

$$-a/R^3 - b = kT\sigma f G\lambda/\eta \tag{57b}$$

which in turn yield $a = -(R^3/3)kT\sigma f G\lambda/\eta$ and $b = -(2/3)kT\sigma f G\lambda/\eta$. There results

$$v_r = -(2/3)(kT\sigma f G\lambda/\eta)(1 - R^3/r^3)\cos\theta \tag{58a}$$

$$v_\theta = (1/3)(kT\sigma f G\lambda/\eta)((R^3/r^3) + 2)\sin\theta \tag{58b}$$

The sphere velocity u (in the +$\hat{\mathbf{x}}$ direction) relative to stationary solution at large distance is determined by applying eq 53c, which yields finally

$$u = (2/3)kT\sigma f G\lambda/\eta \tag{59}$$

Evidently, u is independent of the microsphere radius, R, at constant σ and λ. The surface density of acid groups can be expressed as $\sigma = M/4\pi R^2$, and u can be re-expressed as

$$u = kTMfG/(\zeta_{st}(R/\lambda)) = F_{ch}/\zeta \tag{60}$$

where F_{ch} is the total chemotactic force exerted by the solution on the microsphere and

$$\zeta = (R/\lambda)6\pi\eta R \tag{61}$$

is the associated friction factor (or inverse mobility), which exceeds the usual Stokes friction factor by the ratio R/λ. Unfortunately, the σ (or M) values of the microspheres studied by Zheng and Pollack were not reported and may not have been available in any case. Nowadays, $A_{ch} = 1/\sigma$ is often reported as the "parking area", and typical values for carboxyl microspheres with $R = 1.0$ nm lie in the range $A_{ch} = 14$–100 Å^2, although values as low as 6 and as large as 150 Å^2 have been advertised. It was noted that true close packing of surface

dx.doi.org/10.1021/jp302587d | J. Phys. Chem. B 2013, 117, 7626–7652

carboxyl groups requires $A_{ch} \geq 20$ Å^2, and significantly smaller experimental values were attributed to availability of subsurface sites.[60]

The Unknown Value of λ. No measured values of λ for water in contact with polymer microspheres have been reported. Even for water in contact with glass, a consensus value is lacking. The most precise measurements of λ for polished glass yield $\lambda = 26-57$ nm,[61] but other less precise measurements indicate that $\lambda \leq 1$ nm for plain pyrex and other possibly unpolished glass surfaces.[62] The value of λ typically decreases with increasing surface roughness, and highly charged (small A_{ch}) microsphere surfaces appear to be rather rough in the electron micrographs reported by some suppliers. Under the present circumstances, a reliable *a priori* prediction of microsphere velocities is not possible. Instead, we shall adjust a single parameter, namely, the ratio, $\lambda/A_{ch} = \lambda\sigma$, to match the observed velocity in expected gradients, and examine the values of λ implied by various choices of A_{ch}.

The Fluid Velocity Field. Note that the present fluid velocity field differs greatly from that of Stokes flow. The Cartesian components of the fluid velocity in the xy plane of a coordinate frame that translates with the sphere with velocity $\mathbf{u} = u\hat{\mathbf{x}}$ relative to resting fluid at large $r \to \infty$ are given by

$$S_x = v_r \cos\theta - v_\theta \sin\theta + u = (kT\sigma fG\lambda/\eta)(R^3/r^3)(\cos^2\theta - 1/3) \quad (62a)$$

$$S_y = v_r \sin\theta + v_\theta \cos\theta = (kT\sigma fG\lambda/\eta)(R^3/r^3)\sin\theta\cos\theta \quad (62b)$$

These velocities decline as $\sim 1/r^3$ with increasing r, rather than the $\sim 1/r$ falloff of the Stokes velocity, and the angular part of the flow pattern is dipolar, which also differs from Stokes flow. When the azimuthal angle, ϕ, differs from $\phi = 0$, then one has

$$S_y = (kT\sigma fG\lambda/\eta)(R^3/r^3)\cos\theta\sin\theta\cos\phi \quad (62c)$$

$$S_z = (kT\sigma fG\lambda/\eta)(R^3/r^3)\cos\theta\sin\theta\sin\phi \quad (62d)$$

By using the relations $\cos\theta = x/r$, $\sin\theta\cos\phi = y/r$, and $\sin\theta\sin\phi = z/r$, it was confirmed directly that $\nabla^2 S_x = 0 = \nabla^2 S_y = \nabla^2 S_z$, so $\mathbf{S}$ and also $\mathbf{v} = \mathbf{S} - u\hat{\mathbf{x}}$ satisfy eq 49. It was also verified directly that $\nabla\cdot\mathbf{S} = 0$ and $\nabla \times \mathbf{S} = 0$.

Conditions for Validity of eqs 59 and 60. It is assumed in eqs 59 and 60 that cosolute diffusion is sufficiently rapid and u is sufficiently small that the fluid flow associated with the macromolecular motion does not significantly perturb the cosolute gradient. This will be the case if the time, $t_M = R/u$, for the macromolecule to move a distance equal to its radius, R, significantly exceeds the time, $t_{NaOH} = (10R)^2/2D$, for Na^+ and OH^- ions to undergo an rms displacement of 10 macromolecular radii. The diffusion coefficient for NaOH is $D = 2.1 \times 10^{-5}$ cm^2/s. This condition can be expressed as $D/(50R) \gtrsim u$. For macromolecules of radius $R \lesssim 1$ μm (10^{-4} cm), this condition is easily met for macromolecular velocities less than $\sim$40 μm/s (0.0040 cm/s). The microsphere velocities reported by Pollack and co-workers are typically only a few micrometers per second or less, so this condition is satisfied in such cases.

It is also assumed in eqs 59 and 60 that the cosolute binding reaction is sufficiently rapid to maintain equilibrium with the solution surrounding the macromolecule at all times. This condition can be stated as $\ln[c_{OH^-}(x + \tau u)/c_{OH^-}(x)] = \tau u\partial \ln c_{OH^-}/\partial x \leq 0.1$, wherein the re-equilibration time, $\tau = \tau_{diss} + \tau_{bind}$, is the sum of the mean time (τ_{diss}) for dissociation of OH^- from $PCOO^-$ (the reverse step of eq 21) and that (τ_{bind}) for association of OH^- wth PCOOH (the forward step of eq 21). This condition states that the distance moved by the microsphere along the gradient in the time required to undergo a full (dissociation and rebinding) re-equilibration step should result in a change of $\ln c_{OH^-}$ by less than 0.1, which corresponds to a $\leq$10% change in the contribution of the binding reaction to the standard state chemical potential of the macromolecule. For reaction 21 at the jth site, $\tau_{bind} = 1/(\vec{k}c_{OH^-})$ and $\tau_{diss} = 1/\vec{k}$, where $\vec{k}$ is the rate constant for the diffusion-controlled bimolecular association step, $\vec{k} = \vec{k}/K_b$ is the unimolecular rate constant for the dissociation step, and K_b is the equilibrium constant (at the midpoint (pH 6.0) of the titration curve) for OH^- binding to a $-$COOH group on a highly charged microsphere. Typically, $\vec{k} = 10^{10}$ M^{-1} s^{-1}, and in this case, $K_b = 10^8$ M^{-1}, so $\vec{k} = 100$ s^{-1} and $\tau_{diss} = 0.01$ s. For $c_{OH^-} = 10^{-6}$ M, one has $\tau_{bind} = 10^{-4}$ s and $\tau = 0.0101$ s. For velocities $u \leq 0.0004$ cm/s, the above equilibration condition will be satisfied for all gradients, $dc_{OH^-}/dx \leq 24750$ cm^{-1}, which likely encompasses all practically attainable gradients. However, if $c_{OH^-} = 10^{-11}$ M, then $\tau_{bind} = 1$ s, and the condition is satisfied for all gradients, $dc_{OH^-}/dx \leq 25$ cm^{-1}, which holds for all times, $t \geq 24$ s, in the experiments of Zheng and Pollack[23] (cf. Table 1), but not at shorter times. This re-equilibration condition becomes much more stringent for much larger K_b, as occurs for more acidic groups such as sulfuryl or sulfonyl groups, as discussed in the subsequent paper II (10.1021/jp302589y).[37] Whenever this condition fails, the velocities computed according to eqs 59 and 60 will overestimate the actual velocity. Since carboxylated microspheres are considered here only at pH $\geq$ 3, and the observed velocities are in any case $\leq$0.0001 cm/s, the equilibration condition holds for all but the very shortest times (the first several seconds).

Table 1. Hydroxide Concentration Gradient and Velocity of a Microsphere with $\lambda/A_1 = 2.02 \times 10^6$ at $x = x_0$ at Various Times

t (s)	$d\ln c_{OH^-}/dx$ (cm^{-1})	u (μm/s)	λ/A_1[a] (cm^{-1})	A_1[b] (Å^2)	λ[c] (Å)
20	27.53	1.5	2.02×10^6	10	0.20
200	8.71	0.47	2.02×10^6	10^2	2.02
2000	2.75	0.15	2.02×10^6	10^3	20.2
20 000	0.87	0.05	2.02×10^6	10^4	202.0

[a] λ/A_1 is independent of t. [b] Assumed value of area per surface group, A_1, independent of t. [c] Value of slip length, λ, implied by the constraint $\lambda/A_1 = 2.02 \times 10^6$ and the choice of A_1, also independent of t.

In the case of amidinated spheres, the relevant reaction is given by eq 38 with $P-NH_2$ replaced by $P-C(NH)NH_2$ and $P-NH_3^+$ replaced by $P-C(NH_2)_2^+$. In this case, the equilibrium constant at the midpoint of the titration curve, which is estimated to lie near pH 11.0 (after applying a downward shift of $\sim$1.50 to the intrinsic p$K_a \simeq$ 12.50, due to electrostatic interactions), is $K_a \simeq 10^{11}$ M^{-1}. The relevant condition in this case is $\tau u\partial \ln c_{H^+}/\partial x \leq 0.1$, where now $\tau_{bind} = 1/(\vec{k}c_{H^+})$, $\vec{k} \cong 2 \times 10^{10}$ M^{-1} s^{-1}, $\vec{k} = \vec{k}/K_a = 0.2$ s^{-1}, and $\tau_{diss} = 1/\vec{k} = 5.0$ s. For $c_{H^+} = 10^{-4}$ M, one has $\tau_{bind} = 5 \times 10^{-7}$ s and $\tau \simeq 5.0$ s. For velocities $u \leq 0.0004$ cm/s, the equilibration condition will be satisfied when $\partial \ln c_{H^+}/\partial x \leq 50$ cm^{-1}, which is the case for all times, $t \geq 6$ s, in the experiments of Zheng and Pollack. If $c_{H^+} = 10^{-10}$ M, then $\tau_{bind} = 2.0$ s and $\tau = 7.0$ s. In this case, the equilibration condition becomes $\partial \ln c_{H^+}/\partial x \leq 36$

dx.doi.org/10.1021/jp302587d | J. Phys. Chem. B 2013, 117, 7626−7652

cm^{-1}, which holds for all times $t \geq 12$ s in the experiments of Zheng and Pollack. For the somewhat smaller observed velocities $u \leq 0.0001$ cm/s, this equilibration condition is satisfied over a broad range of pH at all but the earliest times (the first several seconds).

General Comments Regarding the Induced Velocity. If spherical macromolecules exhibit a constant surface density of carboxyl (or amino) groups and a constant slip length, regardless of size, then the number of such groups scales as $M \sim R^2$, so the force scales as $F \sim R^2$, yet the velocity should scale as R^0 (i.e., u should be independent of R) under the same conditions of cosolute concentration and gradient.

We now consider microspheres of radius R, bearing carboxyl groups with average area, A_{ch}, per carboxyl group, hence, $M = 4\pi R^2/A_{ch}$. We assume that $c_{OH^-} \geq 10^{-7}$ M, so $f \cong 1.0$, and that $c_{salt} \simeq 0$, so $c_{OH^-}/(c_{salt} + c_{OH^-}) \simeq 1.0$. We also neglect the W term $(0 \leq W \leq 2)$ in eq 33, even though it might equal or exceed the first term. Hence, the calculated u will be a lower bound. If $A_{ch} = 10^{-12}$ cm^2 and the sodium hydroxide concentration exceeds 0.01 M, then W should be less than 0.14, so neglect of the W term in G of eqs 51, 59, and 60 yields an accurate estimation of u in this case. However, for an electrolyte concentration, $c_S \approx 10^{-5}$ M, which is a lower bound at pH 8.0 in the presence of adventitious CO_2, and for any $A_{ch} \leq 10^{-12}$ cm^2, W should lie between 1.6 and 2.0, unless the distribution of carboxyl groups is highly non-uniform, which is most likely the case. In that event, an accurate NLPB calculation for the actual (presently unknown) distribution of intrinsic charges would be required for a precise estimation of W. When W is neglected, the lower bound induced velocity is given by

$$u = (2/3)(kT/\eta)(\lambda/A_{ch})(\mathrm{d} \ln c_{OH^-}/\mathrm{d}x)_{T,P,c_P^\infty,c_{salt}} \quad (63)$$

At $T = 293$ K, the viscosity of water is $\eta = 0.01$ P (cgs) or 0.001 Pa s (mks). Induced velocities are calculated by eq 63 for a selection of hydroxide gradients in the next section.

SPECIFIC PREDICTIONS AND COMPARISONS WITH EXPERIMENT

Relevant OH^- Gradients and Velocities and First Estimate of λ/A_{ch}. Induced microsphere velocities have been observed in both stationary[18] and temporally evolving salt gradients.[21,22] However, as far as we know, induced microsphere velocities have not been investigated previously in stationary hydroxide gradients but only in time-dependent hydroxide gradients that evolve from particular initial conditions. A diagram of a suitable initial cosolute concentration profile is shown in Figure 3. The initial concentration is higher in the exterior regions ($x < x_0$ and $x > x_0$) and far lower in the interior region ($-x_0 \leq x \leq x_0$). The solutions to the diffusion equation in regions A ($x_0 < x \leq \infty$) and B ($0 \leq x \leq x_0$) are derived in Appendix C, and are presented in eqs C17 and C18. The gradient, $\mathrm{d} \ln c_A(x, t)/\mathrm{d}x$, for cosolute in region A is readily found to be

$$\begin{aligned}\mathrm{d} \ln c_A(x, t)/\mathrm{d}x &= (1/c_A(x, t))\mathrm{d}c_A(x, t)/\mathrm{d}x \\ &= \{c_A + ((c_B - c_A)/2)(\mathrm{erfc}[(x - x_0)/\sqrt{4Dt}] \\ &\quad - \mathrm{erfc}[(x + x_0)/\sqrt{4Dt}])\}^{-1} \\ &((c_A - c_B)/(4\pi Dt)^{1/2})(\exp[-(x - x_0)^2/4Dt] \\ &- \exp[-(x + x_0)^2/4Dt]) \quad (64)\end{aligned}$$

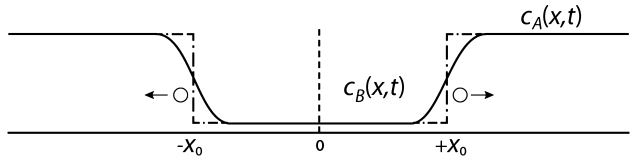

Figure 3. Cosolute concentration profiles at times 0 and t. The dash-dot-dash line denotes the initial ($t = 0$) cosolute profile with concentration c_A in region A ($-x_0 \leq x \leq +x_0$) and c_B in regions B ($x < x_0$; $x > x_0$). This approximates the actual initial profile, when a slab of gel with cosolute concentration c_A is immersed in a solution with concentration c_B. The solid line denotes the cosolute concentration profile after the passage of some time t, when the profile is significantly broadened by diffusion. The cosolute diffusion coefficient is assumed to be the same in both the gel and the solution, as found by Schantz and Lauffer.[35] Expressions for $c_A(x, t)$ and $c_B(x, t)$ are derived in Appendix D.

In the limit $x_0 \gg 4Dt$, we have $\mathrm{erfc}[(x_0 + x)/(4 + Dt)^{1/2}] \to 0$ and $\exp[-(x_0 + x)^2/4Dt] \to 0$ for x in the range $x_0 \leq x \leq \infty$. The resulting expressions for $c_A(x, t)$, $\mathrm{d}c_A(x, t)/\mathrm{d}x$, and $\mathrm{d} \ln c_A(x, t)/\mathrm{d}x$ are precisely those expected for an initial step-function concentration profile in an infinite space with the step at $x = x_0$, which provides an important check on eq 64.

In the examples treated in this study, the initial concentration profile is obtained by immersing a gel in a solution. The gel will occupy region B, where $-x_0 < x \leq x_0$. The gel prevents mixing by inhibiting convection on its side of the boundary, and enables the formation of a fairly sharp initial "step" in concentration. We make use of the fact that diffusion coefficients of small cosolutes in dilute aqueous gels are practically the same as in dilute solution.[35] In this first example, we reckon the slope, $\mathrm{d} \ln c_{OH^-}(x, t)/\mathrm{d}x$, at $x = x_0$ for different times after the immersion event, when the gel (region B) is immersed in a solution occupying region A (in which extremely dilute microspheres are suspended). The temperature is $T = 293$ K, and the diffusion coefficient of NaOH is $D = 2.1 \times 10^{-5}$ cm^2/s. It is assumed that $c_{OH^-} \geq 10^{-6}$ M, so $f \cong 1.0$. The gel is assumed to have no intrinsically charged groups. We assume that $x_0 \gg (4Dt)^{1/2}$ for all times considered in this example. Values of the gradient, $\partial \ln c_{H^-}/\partial x$, and the induced velocity, u, are computed according to eqs 63 and 64 at various times for a particular choice of the parameter, λ/A_{ch}. For these calculations, it is assumed that $c_B \cong 0$ (i.e., $c_{OH^-} \cong 0$) at $t = 0$ in the gel. The value of $c_A = c_{OH^-}$ at $t = 0$ in the solution then cancels out of the results, which are presented in Table 1. All velocities are computed at $x = x_0$, where the gradient is maximal. By assuming that $\lambda/A_{ch} = 2.02 \times 10^6$ cm^{-1}, a velocity, $u = 1.5$ μm/s, comparable to that reported by Zheng and Pollack,[23] was computed for $x = x_0$ at $t = 20$ s. The variation of u with time, and also the values of λ implied by different choices of A_{ch} together with the constraint, $\lambda/A_{ch} = 2.02 \times 10^6$ cm^{-1}, are exhibited in Table 1.

The gradient, $\partial \ln c_{H^-}/\partial x$, and u both decline by about 3-fold for every decade increase in time. The slip lengths, $\lambda = 20.2$ and 202 Å, implied by the choices, $A_{ch} = 10^3$ and 10^4 $Å^2$, respectively, can probably be ruled out as being much too large for such a rough largely hydrophilic surface. Moreover, there apparently is no literature precedent for such large A_{ch} values for carboxylated polymer microspheres. These considerations suggest that, for the carboxylated microspheres used by Zheng and Pollack, λ lies in the range 0.2 Å $\leq \lambda \leq$ 2.0 Å and A_{ch} lies in the range 10 $Å^2 \leq A_{ch} \leq 100$ $Å^2$. The latter range appears to be

dx.doi.org/10.1021/jp302587d | J. Phys. Chem. B 2013, 117, 7626−7652

consistent with the limited available data for commercial samples of carboxylated polymer microspheres.

Comparison of Predicted and Observed Microsphere Trajectories and Second Estimate of λ/A_{ch}. We now calculate the temporal trajectory for the displacement, $\Delta(t) \equiv x(t) - x_0$, of a microsphere from x_0 in region A of Figure 2. The situation is the same as in the previous section, where a non-ionic gel occupies region B, $-x_0 \le x \le -x_0$, and the charged microspheres are suspended in region A, $-x_0 \le x < \infty$. The microsphere velocity can be written as $u = dx(t)/dt = d\Delta(t)/dt$ and combined with eqs 59 and 64 to yield a differential equation for $\Delta(t)$

$$d\Delta(t)/dt = (2/3)(kT/\eta)(\lambda/A_{ch}) \{c_A + ((c_B - c_A)/2)(\mathrm{erfc}[\Delta(t)/\sqrt{4Dt}] - \mathrm{erfc}[2x_0 + \Delta(t)/\sqrt{4Dt}])\}^{-1} ((c_A - c_B)/(4\pi Dt)^{1/2}(\exp[(\Delta(t))^2/4Dt] - \exp[(2x_0 + \Delta(t))^2/4Dt])) \quad (65)$$

The initial OH^- concentration inside the gel is assumed to be $c_B = 10^{-8}$ M, which corresponds to pH 6.0, in this example. The non-ionic poly(vinyl alcohol) gels of Zheng and Pollack[23] were stored in aqueous solutions of pH ~5.7 prior to immersion in the microsphere suspension, and pH 6.0 is a reasonable approximation to that. The OH^- concentration of the suspension of carboxylated microspheres is taken to be $c_A = 10^{-6}$ M (pH 8.0), at which point the carboxyl groups are almost completely titrated, so $f \cong 1.0$, as was assumed in eqs 63 and 65. As in the previous section, the salt concentration is assumed to be negligibly small, and the W terms in eqs 31, 50, 51, and 59 are again neglected. When W is neglected, the force on a microsphere of a given charge is underestimated by a factor of 1.0–3.0, depending upon conditions.

The adopted parameters are $T = 293$ K, $\eta = 0.01$ P (cgs), $R = 1.0 \times 10^{-4}$ cm (1.0 μm), $D = D_{NaOH} = 2.1 \times 10^{-5}$ cm^2 s^{-1}, and $\lambda/A_{ch} = 2.83 \times 10^6$ cm^{-1}. If $A_{ch} = 50$ Å^2, then $M = 2.51 \times 10^7$, $\lambda = 1.41$ Å, and all three values are plausible for the carboxylated microspheres of Zheng and Pollack.[23] The value of x_0 was taken to be 0.025 cm, so that the gel "diameter" is $2x_0 = 0.05$ cm, as stated by Zheng and Pollack. $\Delta(t)$ was assumed to be 0 at time $t = 3$ s, in order to avoid the singular behavior at $x = x_0$, when $t = 0$. Then, eq 65 was solved numerically for $\Delta(t)$ over the intervals from $t = 3$ to 300 s and from $t = 3$ to 7200 s by using the Mathematica NDSolve command. The results are displayed in Figure 4.

The displacement, $\Delta(t)$, is about 100 μm at $t = 300$ s. This value was reported by Zheng and Pollack[23] for their experimental model A, which corresponds to the initial concentration profile in Figure 3. Indeed, the value of $\lambda/A_{ch} = 2.83 \times 10^6$ cm^{-1} was determined (by trial and error) to match this reported result. From 300 to 1800 s, $\Delta(t)$ rises a bit further to 120 μm, but the rate of change of $\Delta(t)$ is very slight at longer times. Such behavior might suggest to an unwary observer that the phenomenon of microsphere exclusion from the gel surface has reached a true equilibrium but that conclusion would be entirely incorrect. The contribution of microsphere diffusion to eventually restore equilibrium (after the $d \ln c_{OH^-}/dx$ gradient has died away) has been omitted in our calculations, which span 7200 s (2 h). The microsphere diffusion coefficient is $D_s = kT/6\pi\eta R = 2.5 \times 10^{-9}$ cm^2 s^{-1}, and the time for a microsphere diffuse to a root-mean-squared displacement, $d = 0.012$ cm (120 μm), is $t = \langle(0.012)^2\rangle/2D = 33\,490$ s, which is about 9.3 h. This is ~19 times longer than the ~1800 s (0.5 h) required for the OH^- gradient force to move the microspheres from $\Delta = 0$ to $\Delta = 0.012$ cm (120 μm), and justifies the neglect of microsphere diffusion up to that point. The estimated backfilling time of ~9.3 h is consistent with the observation of Zheng and Pollack[23] that "the exclusion zone persisted easily for hours".

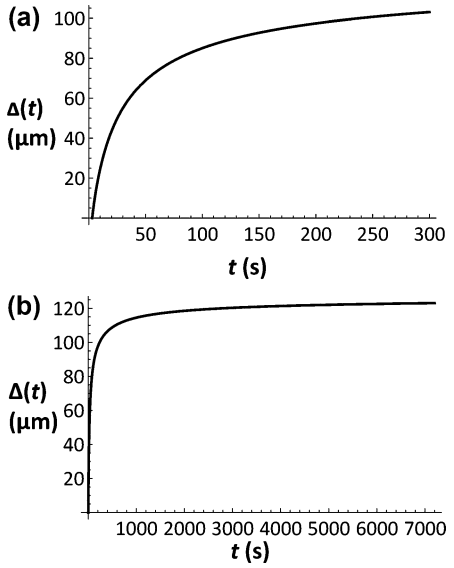

Figure 4. Microsphere displacement, $\Delta(t) \equiv x(t) - x_0$, in a temporally evolving cosolute concentration gradient vs time t after immersion of gel containing $c_A = 10^{-8}$ M NaOH in a solution containing 10^{-6} M NaOH. The trajectory begins at $t = 3$ s with the microsphere at the gel surface at x_0. The trajectory is calculated by numerical integration of eq 65 with $T = 293$ K, $\eta = 0.01$ P, $D = 2.1 \times 10^{-5}$ cm^2/s, and $\lambda/A_1 = 2.83 \times 10^6$ cm^{-1}. (a) Trajectory from $t = 3$ to 300 s; (b) trajectory from $t = 3$ to 7200 s.

It is unfortunate that a more determined effort was not made to ascertain whether the "exclusion zones" were truly equilibrium phenomena, or instead were long-lived non-equilibrium transients. In order to be certain that long-lived concentration gradients are not involved, it would be necessary to observe the system for times that are several-fold greater than the 9.3 h noted above in the case of non-ionic poly(vinyl alcohol) gels. In the case of ionic gels, the situation is more complex, because ion exchange and Donnan effects may influence both the magnitude and evolution of the OH^- or H^+ gradients, as discussed in paper II (10.1021/jp302589y).[37] In such cases, still longer waiting times, sufficient for equilibration of the ion exchange process, will be required to achieve equilibrium.

The trajectories of the same microspheres beginning with different initial displacements, $\Delta(0) = 0$, 60, 120, 180, and 240 μm, at time $t = 3$ s were also computed, and the results are presented in Figure 5. The steepness of these trajectories declines somewhat with increasing $\Delta(0)$, and the net displacements $(\Delta(300) - \Delta(0))$ from the different starting positions at $t = 300$ s are 103, 95, 90, 80, and 75 μm for, respectively, $\Delta(0) = 0$, 60, 120, 180, and 240 μm. It is perhaps surprising that, despite such different starting positions, the differences in net displacement along each trajectory at $t = 300$ s are so modest. This is due to the fact that the force is proportional to $d \ln c_{OH^-}/dx$, rather than simply to dc_{OH^-}/dx. Zheng and Pollack[23] noted that microspheres at very different

dx.doi.org/10.1021/jp302587d | J. Phys. Chem. B 2013, 117, 7626–7652

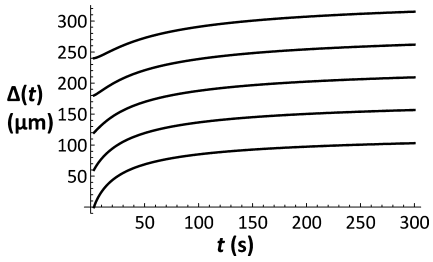

Figure 5. Microsphere displacements $\Delta(t)$ in a temporally evolving cosolute concentration gradient vs time t after immersion of gel containing containing $c_A = 10^{-8}$ M NaOH in a solution containing 10^{-6} M NaOH. The trajectories are computed using the same parameters as in Figure 4. These trajectories all begin at the same time, $t = 3$ s, but at different initial displacements, $\Delta(0) = x(0) - x_0$, which are from bottom to top: $\Delta(0) = 0$ μm; $\Delta(0) = 60$ μm; $\Delta(0) = 120$ μm; $\Delta(0) = 180$ μm; $\Delta(0) = 240$ μm. The lowermost curve is that in Figure 4a.

initial positions, ranging from ∼0 to 250 μm from the gel surface, exhibited surprisingly similar trajectories of their net displacements ($\Delta(t) - \Delta(0)$). That observation was used to argue that a pH gradient could not be responsible for the microsphere translations leading to formation of the exclusion zone. However, the computed trajectories in Figures 3 and 4 demonstrate clearly that a pH gradient can qualitatively, and almost quantitatively, reproduce the observed trajectories of microspheres with a plausible (assumed) value of λ/A_{ch} for a whole range of starting positions from 0 to 240 μm from the gel surface. The modest difference between the $\lambda/A_{ch} = 2.83 \times 10^6$ cm^{-1} required to yield the observed $\Delta(300) = 100$ μm and the $\lambda/A_{ch} = 2.02 \times 10^6$ cm^{-1} required to yield $u = 1.5$ μm/s at $t =$ 20 s may be due to an error in our estimated time for which the reported value, $u = 1.5$, applies. Moreover, stirring of the solution during immersion of the gel will slightly broaden the initial step function in base concentration, which in turn will diminish the chemotactic force at x_0 at short times. That will cause a relatively larger reduction in velocity and displacement at short times than at much longer times.

Estimated Values of λ for Microspheres and BSA. The value $\lambda/A_{ch} = 2.83 \times 10^6$ cm^{-1} was obtained by neglecting the W term in eqs 51, 59, and 60. Under the prevailing low ionic strength conditions, it is likely that $\Gamma_{1S}(P(COO^-)_N) \sim 0$ and $\partial\Gamma_S(P(COO^-)_N)/\partial N \sim 0$, in which case $W \sim 2.0$. In this event, the value of G would be approximately tripled, and the value of λ/A_{ch} required to yield the same trajectory would be reduced by 0.33-fold to $\lambda/A_{ch} = 9.4 \times 10^5$ cm^{-1}. If $A_{ch} = 50$ Å^2/group, as assumed before, then $\lambda = 0.47$ Å.

Although estimates of λ for other charged polymer microspheres are lacking, an estimate of λ for BSA in a pH 2.2 phosphate buffer, where the protein has 92 protonic charges, is obtained in Appendix D. There the present theory is applied to analyze the measured cross-diffusion coefficients, D_{31} and D_{32}, of BSA (component 3) with, respectively, the H_3PO_4 (component 1) and KH_2PO_4 (component 2) of a two-component buffer.[38] Fitted values of the two adjustable parameters were $W = 0.59$ (+0.20, −0.21) and $\lambda = 0.72 \pm 0.28$ Å, which is roughly comparable to the λ estimated for the microspheres. This finding suggests that the slip lengths for the charged microsphere and charged BSA surfaces do not differ greatly. It is perhaps not too surprising that the surface of a glassy copolymer of styrene and a short chain monoacid, such as acrylic or methacrylic acid, in the microspheres and a folded peptide chain in a globular protein have roughly comparable slip lengths. This comparison may lend some credence to the estimates of λ/A_{ch} and λ for the microspheres.

Comparisons of the Theory with Other Observations Involving Non-Ionic Gels. (1) When the initial OH^- concentration is the same in both the gel and microsphere suspension, so $c_A = c_B$, one has $d \ln c_{OH^-}/dx = 0$, and the present theory predicts that $d\Delta(t)/dt = 0$. In this case, there should be no net microsphere motion and no "exclusion zone". Zheng and Pollack[23] varied the pH of the microsphere suspension, and found that no exclusion zone was formed when its pH matched that of the gel (5.7). This was true for both carboxylated (negatively charged) and amidinated (positively charged) microspheres.

(2) When the initial OH^- concentration c_A in a carboxylated microsphere suspension is less than that of the gel ($c_B = 5.0 \times 10^{-9}$ M (pH 5.7)), then $d \ln c_{OH^-}/dx$ is negative, and the force and induced microsphere velocity should be directed inward toward the gel. However, carboxylated microspheres have lost half their charge (i.e., $f = 0.5$) by pH ∼6, and will be even further discharged at lower pH, so f declines and the magnitude of the induced inward velocity may be rather small, and continue to fall with decreasing c_A. Thus, the prediction for suspension pH < 5.7 is for either slow *inward* motion and consequent accumulation of carboxylated microspheres at the gel surface or no perceptible directed motion. Unfortunately, no results for this situation ($c_A < c_B$) were reported, so this prediction remains untested.

(3) When the initial OH^- concentration in the gel is very much less than that in a carboxylated microsphere suspension, so $c_B \ll c_A$, the present theory predicts that $d \ln c_{OH^-}/dx$ is practically independent of both c_A and c_B, provided that the c_{OH^-} experienced by the microspheres is sufficiently great ($c_{OH^-} \geq 10^{-6}$ M (pH 8.0)) to maintain $f \cong 1.0$. Thus, this theory predicts that the temporal trajectory of $\Delta(t)$, and "exclusion zone" size at any given time t, should nearly be independent of the initial pH of the microsphere suspension for any pH at or above pH 8.0. In fact, the data in Figure 10 of Zheng and Pollack[23] show a constant "exclusion zone" size from pH ∼7.8 to ∼10.3 for carboxylated spheres of three different sizes. However, an abrupt increase in "exclusion zone" size was observed when the pH of the microsphere suspension was increased above pH 11.0. This increase is likely due to the fact that −OH groups of the PVA gel react with OH^- above pH 11.0 to become ionized to negatively charged $-O^-$ groups). This process consumes OH^- from the microsphere suspension until the gel is uniformly ionized to an extent that depends upon the c_{OH^-} of the microsphere suspension, the concentration, c_0, of titratable −OH groups in the gel, and the shape of their collective titration curve. The extent of titration of −OH groups of the gel rises with increasing c_{OH^-} of the microsphere suspension. Thus, for pH $\gtrsim$ 11.0, consumption (binding) of OH^- by the gel acts to enhance the diffusive transport of OH^- from the microsphere suspension into the gel. This in turn leads to a larger OH^- deficit in the suspension near the gel, a greater outward gradient, $d \ln c_{OH^-}/dx$, and a larger exclusion zone, as observed by Zheng and Pollack.[23]

(4) For microspheres with the same area per −COOH group, A_{ch}, and slip length, λ, the induced velocity at a given time and position in the gradient is predicted to be independent of microsphere radius, R, so the exclusion zone size at any particular time should also be independent of R. The observations of Zheng and Pollack follow this prediction in the

dx.doi.org/10.1021/jp302587d | J. Phys. Chem. B 2013, 117, 7626−7652

case of carboxylated microspheres with R = 0.45 and 1.0 μm, but similar microspheres with R = 4.0 μm exhibit an exclusion zone size that is 2.4- to 2.8-fold larger than the others in the pH range 8.0−10.5. This deviation from predicted behavior may result from a variation in A_{ch} or λ, or both with sphere size. Surface roughness would be expected to vary, if at all, inversely with R, which would lead to either the same or increased λ, velocity, and exclusion zone size with increasing R, in qualitatitve agreement with the experiments. It is also possible that A_1 is for some reason smaller for the microspheres with larger radii. In the case of amidinated spheres with R = 0.5 and 1.5 μm, the exclusion zone sizes are similar at pH 4.5 and 4.0 but diverge at lower pH with the larger spheres being more excluded. Conceivably, this difference is due to greater availability in the larger spheres of subsurface amidine sites, which are believed by at least one supplier to occur and to become protonated at low pH.

(5) When microspheres bearing protonated amidine groups on their surfaces are employed, eqs 64 and 65 again apply, except that D is now taken to be the diffusion coefficient for HCl. Provided that the c_{H^+} concentration of the microsphere suspension is much greater than that ($10^{-5.7}$ M) in the gel, the resulting trajectories are predicted to be qualitatively similar to those for carboxylated spheres with c_{OH^-} much greater than that ($10^{-8.3}$ M) in the gel, which were described above. This prediction matches the observations of Zheng and Pollack.[23]

(6) When the initial H^+ concentration, c_A, of an amidinated microsphere suspension is less than that of the gel ($c_A = 2 \times 10^{-6}$ M (pH 5.7)), then $d \ln c_{H^+}/dx$ is negative, and the force and induced microsphere velocity should be directed inward toward the gel. The pK_d of a protonated amidine is ~12.4, so amidinated spheres should be nearly fully charged up to pH ~ 10.0. Thus, when the pH of the amidinated microsphere suspension lies in the range 7.0 to ~10.0, the microspheres are predicted to move toward the gel surface, and to accumulate in concentrated layers around the gel (if it is impenetrable to the microspheres). Experimental results for this situation were not reported, so this prediction remains untested.

The predictions for non-ionic gels in the absence of salt are simpler and more direct than those for charged gels. Hence, the predicted attraction or non-exclusion of carboxylated spheres in suspensions with pH < 5.7, and the predicted attraction of amidinated spheres in suspensions with 7.0 $\lesssim$ pH $\lesssim$ 10.0, when the non-ionic PVA gel is pre-equilibrated with pH 5.7 distilled water, should allow rather direct experimental tests of the present molecular chemotaxis theory.

The Effect of Salt on Exclusion Zone Size. The total force on a microsphere bearing carboxyl groups in the presence of salt is given by eqs 33−35. The effect of including salt in the microsphere suspension (but not in the gel) is to decrease the factors $c_{OH^-}/(c_{salt} + c_{OH^-})$ and W in eq 31 but to increase $c_{salt}/(c_{salt} + c_{OH^-})$ while decreasing W in eq 32. If $d \ln c_{salt}/dx \approx d \ln c_{OH^-}/dx$, as would be expected in this case, then the opposing effects of salt on $c_{OH^-}/(c_{salt} + c_{OH^-})$ and on $c_{salt}/(c_{salt} + c_{OH^-})$ effectively cancel, and the primary effect of salt is simply to reduce W. Thus, a decrease in the total force is expected, but even if W were to decrease all the way to zero, the 1 term in the curly braces of eq 31 would remain. Consequently, this theory predicts a moderate relative decrease in size of the exclusion zone (at a given time) around a non-ionic gel upon addition of salt to the microsphere suspension. This prediction agrees with the observations of Zheng and Pollack (cf. their Figure 7).[23]

Convection Induced by Chemotactic Forces. We undertook initial experiments to investigate microsphere motions in gradients of more macroscopic extent than those prevailing in the experiments of Pollack and co-workers. Straight channels with poly(dimethylsiloxane) (PDMS) sidewalls and glass bottoms that were 2 mm wide, 4 mm deep, and 1 cm long were filled to a depth of 2 mm with a homogeneous suspension containing both 1 μm diameter carboxyl microspheres and 3 μm diameter amine microspheres. The gradient was formed by placing a cylindrical agarose gel (4 mm high, 3 mm in diameter), which had been equilibrated with a particular concentration of NaOH (e.g., 0.1, 0.01, or 0.001 M), into a well at one end of the channel and a corresponding cylindrical gel that had been equilibrated with the same concentration of HCl into a well at the other. Microsphere motion was observed through an inverted microscope. Invariably, any motion of the microspheres relative to the fluid was eventually overwhelmed by convection of the visible bottom layer of the solution toward the acidic end of the channel. Finally, we realized that such behavior should have been expected for the following reason.

The chemotactic forces in eqs 31−35 are exerted by a solution exhibiting a pH and/or salt gradient upon a macromolecule bearing acid or base groups. According to Newton's third law, the macromolecule exerts an equal and opposite force on the solution. If the ionized microspheres in such a solution were fixed, the solution would then move in the opposite direction to that taken by free microspheres. The glass bottom of the channel bears ionized silanol groups (except at low pH), and consequently would be expected to exert a force on any solution exhibiting a pH gradient so as to induce convection of its bottom layer toward the acidic end of the channel.

In order to develop a simple approximate theory of chemotactically induced flow, we considered a channel with a uniform rectangular cross section, whose length far exceeds its rather shallow depth. The flat horizontal bottom of the channel is glass bearing many acid silanol groups, but the vertical side walls of the channel are plastic and should bear no ionizable groups, and the top of the channel is uncovered and exposed to air. When the channel is filled to a depth z_0 with solution containing a positive gradient of NaOH and/or salt in the $+x$ direction along the channel axis, the solution will experience a force in the $-x$ direction that originates from its interaction with the channel bottom. The resulting chemotactically induced convection is analyzed in an approximate way in Appendix E. Important simplifying assumptions are invoked. In particular, it is assumed that (i) a quasi-steady-state flow exists at early (but not too early) times before the induced non-uniform flow (due to non-uniform surface ionization) significantly alters the initially uniform solution depth and gradient of $\ln c_{NaOH}$ along the channel axis; (ii) the sidewalls of the channel exhibit slip boundary conditions, so there is no variation of the x-component of the velocity in a direction (y) perpendicular to the channel axis; and (iii) the range of surface−solution contact interactions is $1/h \sim 10^{-9}$ cm. Both no slip (stick) and partial slip boundary conditions at the bottom glass−solution interface were considered, but the former yielded insignificant velocities, $0 \geq v_x \geq -1.97 \times 10^{-2}$ μm/s, and will not be discussed further. Values of the slip length (λ) at the water−glass interface (in the case of partial slip) were taken to be λ = 1.0,[62] 26,[61] or 57 nm.[61] The surface density of ionized silanol groups is reckoned for two particular conditions ($c_{NaOH} = 10^{-4}$ and 10^{-5} M) according to the method

dx.doi.org/10.1021/jp302587d | J. Phys. Chem. B 2013, 117, 7626−7652

of Behrens and Grier.[59] For a gradient, $d \ln c_{NaOH}/dx = 18.4$ cm^{-1}, equivalent to a four decade change over 0.5 cm, the computed force on the solution per unit area of glass−water interface was reckoned (with $W = 0$) to be $-kTf\sigma G = -19.7$ dyn cm^{-2}, at the position in the channel where $c_{NaOH} = 10^{-4}$ M, and $-kTf\sigma G = -4.94$ dyn cm^{-2}, at the position where $c_{NaOH} = 10^{-5}$ M. For the former concentration ($c_{NaOH} = 10^{-4}$ M), the induced fluid velocity (except for a very thin region of depth $\sim 1/h = 0.01$ nm near the glass bottom) was estimated to be $v_x(z) \simeq -2.0$ μm/s for $\lambda = 1.0$ nm and $v_x(z) \simeq -51$ or -112 μm/s for, respectively, $\lambda = 26$ or 57 nm. The fluid velocity, $v_x(z)$, is independent of z, except extremely close to the solid−solution interface, so is very nearly plug flow. For the latter concentration ($c_{NaOH} = 10^{-5}$ M NaOH), the induced fluid velocity was estimated to be $v_x(z) \simeq -0.494$ μm/s for $\lambda = 1.0$ nm and $v_x(z) \simeq -12.8$ or -28.2 μm/s for, respectively, $\lambda = 26$ or 57 nm. Even in the event that $\lambda = 1.0$ nm, these predicted velocities are significant, and should be observable under the right conditions. We emphasize that these are not steady-state velocities, because the variation of the force per unit area and flow rate along the channel will soon lead to fluid pile-up, an associated pressure gradient along the channel that at least partially opposes the chemotactic force responsible for the flow, and eventually a counterflow in an upper layer. A complete description of this phenomenon would require a numerical solution of the combined fluid flow and NaOH diffusion equations, together with a simultaneous evaluation of the surface charge density and the total force (per unit area) exerted on the solution by each element of the glass surface taking into account both the NaOH binding and electrostatic contributions at each time step. Such a calculation is not undertaken here, in part because some parameters, such as A_{ch} and λ, are not sufficiently well-known and in part because other mechanisms may also be simultaneously driving convection, as described below.

Convection Induced by a Gradient of Surface Tension. Chemotactically induced convection can be regarded as a particular case of a general phenomenon, wherein a tangential traction is exerted on a fluid surface element by a gradient of the surface tension (surface free energy per unit area), and must be balanced by a viscous (shear) traction exerted on the same surface element by a velocity gradient of the adjacent fluid, which in turn requires convection. So-called Marangoni convection is induced by a gradient of the surface tension at an interface between two fluids, such as an aqueous solution and air, and differs from flow at a solid−liquid interface in the following way. The viscosity of the solid is effectively infinite, and only very slight slippage of the first fluid layer relative to the solid surface is possible in accord with the partial slip coundary condition, so the resulting fluid flow near the interface is effectively plug flow with little or no gradient except between the solid and the first fluid layer. This results in a rather small flow velocity per unit traction. In contrast, for an aqueous solution−air interface, there is virtually no counterbalancing traction on the air side of the interface so a large velocity gradient of the adjacent solution, which is generated by a rapid surface flow, is required to provide the necessary traction to counter the surface tension gradient. A Marangoni convection cell involving a horizontal air−solution interface typically exhibits rapid flow in the direction of the surface tension gradient in a very thin layer near the interface, and a much slower flow in the opposite direction at a somewhat greater depth with the velocity trending to zero at the bottom and sidewalls.[63] Of course, a downward vertical component of the flow at the high end of the surface tension gradient and an upward vertical component of the flow at the low end of the gradient are required to connect the top and bottom horizontal flows. When $\partial \ln c_{NaOH}/\partial x = -18.4$ cm^{-1}, the surface tension gradient, or equivalently the traction experienced by the air−solution interface, at the point where $c_{OH^-} = 10^{-4}$ M is $\partial\gamma/\partial x = -3.0 \times 10^{-3}$ dyn/cm^2, which is $\sim 1.5 \times 10^{-4}$-fold smaller than that ($-kTf\sigma G = -19.7$ dyn/cm^2) due to the chemotactic force on the glass-bottom surface, and at the point where $c_{OH^-} = 10^{-5}$ M, the traction is $\partial\gamma/\partial x = -3.0 \times 10^{-4}$ dyn/cm^2, which is 6.1×10^{-5}-fold smaller than that ($-kTf\sigma G = -4.94$ dyn/cm^2) due to the chemotactic force on the glass-bottom surface. Such small tractions might render the flow due to a Marangoni convection cell in the region below the thin upper layer negligibly small compared to the chemotactic flow in that same region. The surface tension and its gradient at the putatively non-ionic hydrophobic sidewall−solution interfaces should be very roughly comparable to the same quantities at the air−water interface. However, owing to the partial slip boundary condition in this case, the induced flow velocities should be far ($\leq 10^{-3}$-fold) smaller than those induced by the far greater chemotactic forces exerted on the solution by the glass bottom. Thus, for the very dilute ionic solutions and gradients of $\ln c_{OH^-}$ considered here, any contribution of the hydrophobic sidewalls to generate convective flow should be negligible compared to that of the glass bottom. Because γ at the air−solution interface increases with decreasing c_{HCl} and with increasing c_{NaOH},[64] the sign of $\partial\gamma/\partial x$ at the air−water interface of a channel with an NaOH reservoir at its small-x end and an HCl reservoir at its large-x end is everywhere negative, and its associated Marangoni flow of the top surface proceeds from the acidic end toward its basic end, whereas its counterflow below the thin surface layer proceeds in the opposite direction toward the acidic end of the channel. Chemotactically induced flow in the bottom layer is also directed toward the acidic end of the channel, whereas its counterflow proceeds toward the basic end in the upper layer(s). Thus, in principle, convection cells driven by Marangoni flow at the air−solution interface and chemotactically induced flow induced by the glass bottom could reinforce one another, whenever those two flows have comparable strength. Any convection cell with a sufficient fluid velocity toward the acidic end of the channel in the visible lower layer(s) would account for the observed convection in the glass-bottom channels. However, experiments on channels with putatively non-ionic hydrophobic bottoms and sidewalls in the next section suggest that Marangoni tractions in these dilute ionic solutions are too small to cause perceptible convection by themselves.

Preliminary Experiments. Experiments were undertaken to observe microsphere motions in open channels with non-ionic hydrophobic PDMS (poly(dimethyl siloxane) bottom and sidewall surfaces, which were supposed not to cause chemotactically induced convection. Channel dimensions, cylindrical wells, and gel plugs were the same as for the previously described glass-bottom channels. The microsphere solutions contained either 100% or 50 v/v % D_2O to render the microspheres more nearly neutrally buoyant. Six experiments were performed, each using a separate chip upon which a single channel was fabricated. In one experiment, the microsphere suspension was replaced by a solution of pH indicator, phenol red ($pK = 8.0$). A color boundary appeared midway along the channel after 3−5 min and persisted for 20 min without

dx.doi.org/10.1021/jp302587d | J. Phys. Chem. B 2013, 117, 7626−7652

moving, which indicates an absence of significant convection in the visible bottom layer in that channel. In none of these experiments were microspheres observed to be all convected toward either end, in contrast to the convection toward the acidic end that was invariably observed in glass-bottom channels. These findings suggest that, by itself, Marangoni convection in these solutions is too weak to induce significant flow in the visible bottom layer, and that the convection observed earlier in glass-bottom channels was almost entirely due to chemotactically induced flow. The results pertaining to microsphere chemotaxis were encouraging in the sense that the predicted preferential accumulation of carboxyl microspheres toward the basic end of the channel and amino microspheres toward the acidic end was clearly observed in two of the five trials. However, in the other three trials, no significant segregation or directed microsphere motion was apparent and only Brownian motion was observed. The irreproducibility of these experiments, which were each performed using a different channel, likely arises at least in part from unanticipated ionizable silanol groups on the PDMS surfaces due to insufficient recovery of hydrophobicity (by surface reconstruction) after oxygen plasma treatment (for bonding purposes) during the fabrication process. Undetected non-uniform convection due to non-uniform surface charge, fluid pile-up, and backflow at early times in channels with unanticipated ionic surfaces could potentially stir the channel contents sufficiently to greatly diminish the gradients of $\ln c_{OH^-}$ and $\ln c_{OH^+}$ in such channels.

Experiments to investigate a pH-gradient driven convection pump in an open channel of circular topology, specifically a horizontal rectangular loop, were also undertaken. All bottom and side surfaces were intended to be non-ionic hydrophobic PDMS, except along one side of the rectangle, which had a glass sidewall in addition to a basic gel plug in a corner well at one of its ends and an acidic gel plug in a corner well at its other. Convection was probed by suspended fluorescent microspheres. Again, results were encouraging in the sense that the predicted circular flow around all four sides of the rectangular loop (in a direction to move fluid from the basic toward the acidic plug in the side with the glass wall) was observed in one of the three trials. However, no significant flow was apparent in the other two trials, and only Brownian motion was observed. As before, the irreproducibility of these experiments, which were each performed on a different channel, likely stems from unanticipated silanol groups on the PDMS surfaces. Such groups would generate flow toward the acidic plug also in the three sides of the channel loop without the glass wall, and could thereby significantly quench the circular flow generated by the side with the glass wall.

These irreproducibility problems must be resolved in future studies in order to provide reliable tests of the molecular chemotaxis theory.

DISCUSSION

The present theory of the chemotactic force on a single macromolecule suspended in a gradient of dilute small cosolute molecules is based on the variation of its standard state chemical potential with increasing chemical potential of the cosolute species. This slope defines a non-electrostatic preferential interaction coefficient, which is evaluated via Kirkwood−Buff theory, and expressed simply in terms of excluded volume and cosolute−solvent exchange interactions. This preferential interaction coefficient is also evaluated via solution thermodynamics for both non-ionized and electroneutral ionized cosolutes, when the dominant interaction is binding to specific sites on the macromolecule. The modulation of the electrostatic free energy of a charged macromolecule by a monovalent ionized cosolute (electrolyte) is also formally taken into account via an electrostatic preferential interaction coefficient. Chemotactic forces due to thermodynamic binding of NaOH to neutral surface acid groups (carboxyl, silanol) or binding of HCl to neutral surface base groups (amidine, amine) in prevailing gradients of, respectively, $\ln c_{NaOH}$ or $\ln c_{HCl}$ are treated quantitatively. Such ultrashort-range forces generate surface tractions, and the induced velocities are reckoned by a novel hydrodynamic calculation with a partial slip boundary condition. The velocity is proportional to the (unknown) ratio, λ/A_{ch}, of slip length to area per surface group. Trajectories are then computed for microspheres with an optimally adjusted value of λ/A_{ch} in temporally evolving cosolute gradients.

Numerous incisive tests of the present theory of molecular chemotaxis are conducted by comparing its predictions with experiments of Zheng and Pollack pertaining to exclusion of microspheres by non-ionic gels. The present theory accounts qualitatively for essentially all observations pertaining to carboxyl, amidine, and amine microspheres near non-ionic gels. With a single optimally adjusted parameter, λ/A_{ch}, it accounts quantitatively for many of those same observations. A plausible estimate of A_{ch} yields a λ-value for the microspheres which is comparable to that obtained for BSA by fitting the present macromolecular chemotaxis theory to two reported cross-diffusion coefficients between BSA and two buffer components, as described in Appendix E. The present theory correctly predicts neither repulsion nor attraction of carboxyl microspheres, when the internal c_{OH^-} of the gel matches that of its surrounding solution. It likewise predicts correctly that microspheres with amine or amidine groups experience neither repulsion nor attraction, when the internal c_{H^+} of the gel matches that of its surrounding solution. These comparisons with experiment strongly support the present theory of molecular chemotaxis. Verification of the predicted attraction of carboxylated or sulfated microspheres, when the c_{OH^-} of the suspension lies below that of the non-ionic gel, and the predicted attraction of amino or amidinated microspheres, when the c_{H^+} of the suspension lies below that of the non-ionic gel, would flatly contradict any notion that microsphere-excluding long-range ordered water surrounds the gels under such conditions, and would further support the present theory of macromolecular chemotaxis.

Numerous other observations of the Pollack group pertaining to interfaces of ionic gels and ionomers with aqueous solutions are analyzed in a subsequent paper II (10.1021/jp302589y).[22]

Further quantitative testing of the present chemotaxis theory will require additional experiments under conditions where the gradients of $\ln c_{OH^-}$ (or $\ln c_{OH^+}$) and $\ln c_{salt}$ can be independently controlled and/or verified, and will require firm experimental estimates of A_{ch} for the acidic or basic groups on the microsphere surfaces. In addition, detailed NLPB calculations of W (cf. eq 29) will likely be required. Moreover, a complete quantitative test will require independent measurement of λ, which may prove challenging.

The present theory predicts that a solution with a gradient of c_{OH^-} in contact with a smooth glass surface should experience a chemotatic force in a direction opposite to the gradient, so as to place solution with a higher c_{OH^-} in contact with any given patch of surface and thereby lower its total free energy. This

can be regarded as a kind of Gibbs−Marangoni effect arising from a gradient of the surface tension at a fluid−solid interface, which induces convection of the fluid phase, whenever partial slip prevails. The chemotactic force is predicted to induce convection of the solution in the direction of lower c_{OH^-}. This was apparently manifested in our preliminary experiments by persistent convection of the visible bottom layer toward the acid gel plug in straight glass-bottom channels. Replacing glass bottoms with PDMS bottoms evidently reduced convection of the visible bottom layer to imperceptible levels.

Possible Manifestations and Uses of Macromolecular Chemotaxis. *A. Chemotactic Motion of Cells without Swimming Apparatus.* Cell membranes contain both phosphate and carboxylate groups, which can be regarded as neutral acid groups that have bound an OH^-, and retained its charge and also its cation (e.g., Na^+) as a counterion. Thus, a cell in a gradient of OH^- should experience a chemotactic force, and acquire an induced velocity in the direction of greater OH^- concentration. Provided that a cell's typically acidic waste products are not excreted in a spherically symmetric plume, the cell will generally experience an OH^- gradient and a chemotactic force to move it away from its waste products toward a region of greater OH^- concentration. Thus, even a cell lacking cilia, flagellae, or other swimming apparatus is able to move so as to escape its own waste products. Such chemotactic motion may have been important during certain stages of evolution of life on earth, and is conceivably still important for some organisms, and possibly also some organelles.

B. Moving Red Blood Cells through Capillary Beds. Sites that bind ligands in the interior of a cell, as well as those on its surface, may contribute to its chemotaxis, provided that ligand transport from the surface to the interior binding sites is sufficiently rapid. In that case, the interior sites simply increase the effective surface density of sites, $1/A_1$. Chemotactic forces due to binding a single kind of ligand provide no net advantage to cells (e.g., red blood cells) or macromolecules that are used to shuttle ligands from a region of high to a region of low ligand concentration. Because the force is always directed toward a region of high ligand concentration, it opposes the motion toward the low concentration region and provides no net advantage over a full shuttle cycle. In the case of O_2 transport, this problem is "solved" by enabling the hemoglobin and red blood cells to bind a metabolic product ($H^+ + HCO_3^-$), as well as O_2. The numbers of ($H^+ + HCO_3^-$) and O_2 binding sites are identical. Because the chemotactic force generally increases with increasing saturation of the binding sites, the chemotactic force due to O_2 binding (for a given O_2 gradient) is greater in the capillaries of the lung, and lower in those of working muscle tissue, whereas the force due to ($H^+ + HCO_3^-$) binding is greater in the capillaries of working muscle tissue and lower in those of the lung. In working muscle, there is a positive gradient of ($H^+ + HCO_3^-$) and a negative gradient of O_2 across the capillary bed from the arterial to the venous side, so the expected dominant ($H^+ + HCO_3^-$) chemotactic force in this tissue assists or directs the migration of red blood cells across the capillary bed in the proper direction (i.e., from arterial to venous). In the lung, there is a positive gradient of O_2 and negative gradient of ($H^+ + HCO_3^-$) across the capillary bed from the arterial to the venous side, so the expected dominant O_2 chemotactic force in this tissue assists or directs the migration of red blood cells across the capillary bed in the proper direction (i.e., from arterial to venous). Whether such chemotaxis is significant in comparison to pressure-induced flow through the capillary bed is presently unknown, but this possibility merits further investigation.

C. Controlling the Force on DNAs Moving through Nanopores in Membranes. In studies of the passage of either single- or double-strand DNAs and RNAs through pores embedded in membranes, electric fields are typically used to drive the filament through the pore. Often the objective is to analyze the electric current variation as each base of a single-strand DNA passes the main constriction in the pore.[65] In some cases, when the trans-membrane voltage is sufficiently high to produce readily detectable differences in current between each different kind of base, the DNA passes through the pore much too quickly. Hence, a means of retarding the rate of passage of the DNA has been sought.[65] By including a binding species, such as OH^-, on the initial side of the membrane, the net force on the DNA could be varied. The basic idea is that the free energy of a phosphate group is lower in the compartment with the greatest concentration of OH^- (and its counterions). The amount of that free energy lowering divided by the distance, d_P, between phosphate groups is the force pulling the DNA toward the compartment of greatest OH^- concentration. The chemotactic force pulling the DNA toward the initial side can be expressed as

$$\begin{aligned} F &= \Delta\mu_{P1}^{0}/d_P \\ &= (\partial\mu_{P1}^{0}/\partial\mu_{OH^-})_{T,P,c_P^\infty}\cdot\Delta\mu_{OH^-}/d_P \\ &= kTf\ \ln[c_{OH^-}(i)/c_{OH^-}(f)]/d_P \end{aligned}$$

where $\Delta\mu_{P1}^0 = \mu_{P1}^0(i) - \mu_{P1}^0(f)$ is the difference in standard state chemical potential *per phosphate* between the filament in the initial solution and that in the final solution, $(\partial\mu_{P1}^0/\partial_{OH^-})_{T,P,c_P^\infty} = (1.0)f$ is the slope of μ_{P1}^0 with respect to μ_{OH^-} (cf. eq 28 with $M = 1$), and $\Delta\mu_{OH^-} = kT\ln[c_{OH^-}(i)/c_{OH^-}(f)]$ is the difference in chemical potential of OH^- between the final and initial solutions. For an assumed distance, $d_P \simeq 7$ Å, between bases, $f = 1.0$, and a 10-fold ratio of OH^- concentrations, the predicted retarding force is $F \simeq 13$ pN. This could easily be varied by several-fold in either direction by adjusting the OH^- concentrations on either side of the membrane.

D. Chemotactically Induced Convection. A chemotactic fluid pump could have potentially useful microfluidic applications, when ultraslow flow rates are desired. A chemotactically driven rotary motor could also be envisioned, but that lies beyond the scope of the present work.

E. Possible Role of Chemotaxis in Geology. Chemotactic forces may play a modest role in certain geochemical processes, such as transport of suspended charged particles in water with gradients of OH^- and or salt, or percolation of water with such gradients through porous rock or sands that have charged surfaces.[22] Particularly likely places for such processes might be estuarine environments or the aerobic−anaerobic boundary in damp soil, where significant gradients of salt and pH commonly prevail.

F. Possible Use in Fabrication of Nanostructured Materials. Gradients of $\ln c_{OH^-}$ or $\ln c_{OH^+}$ could be used to attract and densify, respectively, carboxyl and amidine microspheres, so as to produce small crystalline arrays. We think that this phenomenon has already been demonstrated inadvertently by the Pollack group,[29] as will be discussed in the subsequent paper II (10.1021/jp302589y). The formation of crystalline arrays of charged (nearly) cylindrical viruses and mixed arrays

of charged species of different shape could also be facilitated in the same manner.

Once the significance of macromolecular chemotaxis of charged macromolecules, colloids, organelles, and cells is recognized, its recorded manifestations and uses are likely to multiply rapidly.

APPENDIX A. EVALUATION OF THE EXCHANGE REACTION CONTRIBUTION

The mean density function for a cosolute center at position $\mathbf{r}_j$ in the jth site on the macromolecule is defined by $P_j^3(\mathbf{r}) = \langle\delta(\mathbf{r} - \mathbf{r}_j)\rangle$, which depends only upon the distance, $r = |\mathbf{r}|$, from the central atom of the macromolecule and should be peaked near the distance $r = \langle|\mathbf{r}|\rangle = \langle|\mathbf{r}_j|\rangle$. The averages are taken first over the positions and configurations (shapes plus orientations in this section) of all 1-molecules and of all other 3-molecules outside the site, then over all positions, $\mathbf{r}_j$, and configurations of the cosolute in the site and over all configurations and orientations of the macromolecule. This density function is automatically normalized so that $\int_V d^3\mathbf{r}P_j^{(3)}(r) = 1.0$ for the jth (and every other) site.

The mean density function for the centers of those 1-molecules that occupy the jth site, when the cosolute is absent, is defined as follows. First, the center of a 3-molecule with fixed configuration is placed at $\mathbf{r}_j$ in the jth site of a 2-molecule with a fixed position and configuration. The density of centers of all η_1 1-molecules in the solution ($\rho_1(\mathbf{r}) = \sum_{l=1}^{\eta_1}\delta(\mathbf{r} - \mathbf{r}_l^1)$) is then averaged over all positions and configurations of those same 1-molecules and of all other 3-molecules. This $\rho_1(\mathbf{r})$ practically vanishes over an excluded volume, $V(\mathbf{r}_j, \xi, \zeta)$, that depends upon the particular $\mathbf{r}_j$ and configurations ξ and ζ of the fixed 2- and 3-molecules, respectively. The quantity $V(\mathbf{r}_j, \xi, \zeta)$ really defines the site for any particular choice of $\mathbf{r}_j$, ξ, and ζ. Now, the 3-molecule is removed (by excluding all states wherein the center of a 3-molecule lies within $V(\mathbf{r}_j, \xi, \zeta)$), but the configuration of the 2-molecule is held fixed at ξ, and the solution is allowed to equilibrate with that. The mean density of those 1-molecules whose centers lie within $V(\mathbf{r}_j, \xi, \zeta)$ is $P_j^1(\mathbf{r}, \mathbf{r}_j, \xi, \zeta) = \langle\sum_{l=1}^{\omega_1}\delta(\mathbf{r} - \mathbf{r}_l^1)\rangle$, where the sum runs only over the ω_1 (variable) 1-molecules in each multi-molecular configuration, whose centers at $\mathbf{r}_l^1$ lie within $V(\mathbf{r}_j, \xi, \zeta)$, and the average is taken over all positions $\mathbf{r}_l^1$ and configurations of all the 1-molecules and those of all the 3-molecules (now excluded from the site) in the solution. This mean density of 1-molecules in $V(\mathbf{r}_j, \xi, \zeta)$ is further averaged over $\mathbf{r}_j$, ξ, and ζ by repeating this process for various $\mathbf{r}_j$, ξ, and ζ and then averaging the results. We obtain finally $P_j^{(1)}(\mathbf{r}) \equiv \langle\sum_{l=1}^{\omega_1}\delta(\mathbf{r} - \mathbf{r}_j)\rangle_{\mathbf{r}_j,\xi,\zeta}$, where the subscripts denote the final averages over $\mathbf{r}_j$, ξ, and ζ. By definition, the average value of ω_1 is $\langle\omega_1\rangle = \int_v d^3\mathbf{r}P_j^{(1)}(\mathbf{r}) = \nu$, where ν is the average number of water molecules in the unoccupied site. In the absence of electrostrictive effects or large volume changes upon mixing 1 and 3, it is expected that $\nu \cong \overline{v}_3/\overline{v}_1$. Finally, rotational averaging of $P_j^{(1)}(\mathbf{r})$ around the central atom of the 2-molecule yields $P_j^{(1)}(r)$, which depends only upon the scalar distance r from that same central atom. The normalization integral is unaffected by the rotational averaging, so $\int_v d^3\mathbf{r}P_j^{(1)}(r) = \nu$. Finally, we note that the contribution of the M identical sites to the pair correlation functions is

$$c_3 g_{32}(r) = f\sum_{j=1}^{M} P_j^{(3)}(r) \tag{A.1a}$$

$$c_1 g_{12}(r) = (1 - f)\sum_{j=1}^{M} P_j^{(1)}(r) \tag{A.1b}$$

Equation 8 can be rewritten as

$$\Gamma_3(2) = c_3\int_0^R d^3r(g_{32}(r) - g_{12}(r)) \tag{A.2}$$

where R is any large value at which $g_{32}(r)$ and $g_{12}(r)$ have converged to 1.0. Substituting eqs 13, A.1a, and A.1b into eq A.2 and making use of the normalization integrals yields the exchange reaction contribution in eq 14 of the main text.

APPENDIX B. THERMODYNAMIC ANALYSIS OF THE BINDING OF IONIC $NA^+ + OH^-$ TO CARBOXYLIC ACID GROUPS

The analysis here follows that in section S3 of the Supporting Information. Although every Na^+ ion is thermodynamically bound to a negative charge, whether an OH^- or $PCOO^-$, it may nevertheless contribute as an independent free particle to lower the solvent chemical potential in a dilute electroneutral solution. However, if a macromolecule, when fully charged (titrated), is a strong polyelectrolyte, then the situation is more complex. Such polyelectrolyte effects are ignored for the moment but are discussed in detail in the main text. The spontaneous reaction of the jth carboxylic acid group is

$$OH^- + PCOOH \rightleftharpoons PCOO^- + H_2O \tag{B1}$$

$PCOO^-$ is an occupied (by an OH^- charge) jth binding site denoted by J_f, and PCOOH is an unoccupied (or empty) jth binding site denoted by J_e, where J denotes the configuration of the $M - 1$ other sites. The overall reaction is the exchange of an incoming OH^- for an outgoing H_2O at the jth binding site. The equilibrium constant is

$$K_b = c_{J_f}^{eq}X_1^{eq}/c_{J_e}^{eq}c_{OH^-} \tag{B2}$$

where c_{J_f} and c_{J_e} are the equilibrium concentrations of, respectively, J_f and J_e, and $X_1^{eq} \cong 1.0$ is the equilibrium mole fraction of solvent water in this dilute solution. The fraction of (OH^- charge) occupied sites is

$$f = K_b c_{OH^-}^{eq}/(1 + K_b c_{OH^-}^{eq}) \tag{B3}$$

and is independent of either site index or configuration J of the remaining $M - 1$ sites. When the jth sites of the macromolecules with configuration J of their $M - 1$ other sites equilibrate their hydroxide binding reactions to reach equilibrium at the prevailing hydroxide and water chemical potentials, $\mu_{OH^-} = \mu_{OH^-}^0 + kT\ln c_{OH^-}^{eq}$ and $\mu_1 = \mu_1^0 + kT\ln X_1^{eq}$, respectively, the changes in numbers and concentrations of the various species are

dx.doi.org/10.1021/jp302587d | J. Phys. Chem. B 2013, 117, 7626−7652

$$J_e: n_J^0 \rightarrow n_J^0(1-f); \qquad c_{J_e}^0 = c_J^0 \rightarrow c_{J_e}^{eq} = c_J^0(1-f)$$

$$J_f: 0 \rightarrow n_J^0 f; \qquad c_{J_f}^0 = 0 \rightarrow c_{J_f}^{eq} = c_J^0 f$$

$$OH^-: n_{OH^-}^0 \rightarrow n_{OH^-}^0 - n_J^0 f; \quad c_{OH^-}^0 \rightarrow c_{OH^-}^{eq} = c_{OH^-}^0 - c_J^0 f$$

$$Na^+: n_{Na^+}^0 \rightarrow n_{Na^+}^0; \qquad c_{Na^+}^0 \rightarrow c_{Na^+}^0$$

$$H_2O: n_1^0 \rightarrow n_1^0 + n_J^0 f; \qquad X_1^0 = 1 - (c_P^0 + 2c_b^0)/c_1^0 \rightarrow X_1^{eq} = 1 - (c_P^0 + 2c_b^0 - c_J^0 f)/(c_1^0 + c_J^0 f)$$

where $c_b^0 \equiv c_{Na^+}^0 = c_{OH^-}^0$. The volume of the solution is assumed to remain constant, unaffected by the reaction. The change in free energy at constant T and P is

$$\begin{aligned}\Delta G_J &= G_J^{eq} - G_J^0 \\ &= n_J^0 f\{\mu_{J_f}^0 + kT\ln[c_J^0 f]\} + n_J^0(1-f) \\ &\quad \{\mu_{J_e}^0 + kT\ln[c_J^0(1-f)]\} - n_J^0\{\mu_{J_e}^0 + kT\ln[c_J^0]\} \\ &\quad + (n_{OH^-}^0 - n_J^0 f)\{\mu_{OH^-}^0 + kT\ln[c_{OH^-}^0 - c_J^0 f]\} \\ &\quad - n_{OH^-}^0\{\mu_{OH^-}^0 + kT\ln[c_{OH^-}^0]\} + (n_1^0 + n_J^0 f) \\ &\quad \{\mu_1^0 + kT\ln[X_1^{eq}]\} - n_1^0\{\mu_1^0 + kT\ln[X_1^0]\} \\ &= n_J^0 kT\ln[1-f] \end{aligned} \tag{B4}$$

The concentrations of the Na^+ ions were omitted, because neither their numbers nor their concentrations change during the equilibration process. The final line of eq B4 was obtained by (1) invoking the equilibrium condition, $n_J^0 f\{\mu_{J_f}^0 + \mu_1^0 - \mu_{J_e}^0 - \mu_{OH^-}^0 + kT\ln[c_{J_e}^{eq} c_1^{eq}/c_{J_e}^{eq} c_{OH^-}^{eq}]\} = 0$; (2) assuming that $c_J^0 \ll c_{OH^-} \ll c_1^0 = n_1^0/V$ and then expanding $\ln[(c_{OH^-}^0 - c_J^0 f)/c_{OH^-}^0] = \ln[1 - c_J^0 f/c_{OH^-}^0] = -c_J^0 f/c_{OH^-}^0$ in the term containing $n_{OH^-}^0$ (but not $n_J^0 f$); and (3) assuming that $c_M^0 + 2c_b^0 \ll c_1^0$ and expanding $\ln[X_1^{eq}] = -(c_P^0 + 2c_b^0 - c_J^0 f)/c_1^0$ and $\ln[X_1^0] = -(c_P^0 + 2c_b^0)/c_1^0$. We then use $c_X^0 = n_X^0/V$ for any species, X, to obtain the last line of eq B4.

The final expression in eq B4 is now summed over all configurations, $J = 1$ to η_J for the particular choice of j, and then over all sites, $j = 1, ..., M$, to obtain the total free energy change associated with the binding reaction

$$\Delta G = \sum_{j=1}^{M}\sum_{J=1}^{\eta_j} n_J^0 kT\ln[1-f] = Mn_P^0 kT\ln[1-f] \tag{B5}$$

The free energy change per macromolecule is

$$(\partial\Delta G/\partial n_P^0)_{T,P,n_1^0,n_{NaOH}^0} = MkT\ln[1-f] \tag{B6}$$

which can be regarded as the contribution of the binding reaction (eq B1) to the standard state chemical potential of the macromolecule, μ_P^0. Finally, the variation of the macromolecular chemical potential with c_{OH^-} (at equilibrium) is given by

$$\begin{aligned}(\partial\mu_P^0/\partial c_{OH^-})_{T,P} &= \frac{\partial}{\partial c_{OH^-}}\left(\frac{\partial\Delta G}{\partial n_P^0}\right)_{T,P,n_1^0,n_{NaOH}^0} \\ &= -MkT\left(\frac{K_b}{1+K_b c_{OH^-}}\right)\end{aligned} \tag{B7}$$

The force on the macromolecule arising from cosolute binding is

$$\begin{aligned}F_b &= -\left(\frac{d\mu_P^0}{dx}\right)_{T,P} \\ &= -\left(\frac{\partial\mu_P^0}{\partial c_{OH^-}}\right)_{T,P}\frac{dc_{OH^-}}{dx} \\ &= MkT\left(\frac{K_b c_{OH^-}}{1+K_b c_{OH^-}}\right)\frac{d\ln[c_{OH^-}]}{dx}\end{aligned} \tag{B8}$$

Equation B8 is identical to eq A8 with c_{OH^-} in place of c_L. It is precisely what would be expected for binding a non-ionic "molecular" NaOH cosolute ligand.

Equations B4–B8 are unaffected by the presence of other non-ionic species whose numbers and concentrations are not affected by the reaction, and which do not alter K_b. However, if a partially or fully titrated form of the macromolecule is a strong polyelectrolyte in the sense that it has a high (compared to kT) electrostatic free energy per intrinsic charge, added electrolyte may substantially lower its electrostatic free energy, and thereby also its standard state chemical potential, as described in the main text.

APPENDIX C. SOLUTION OF THE DIFFUSION EQUATION

The cosolute concentration evolves from the initial profile in Figure 2 according to the diffusion equation

$$\frac{\partial c(x,t)}{\partial t} = D\frac{\partial^2 c(x,t)}{\partial x^2} \tag{C1}$$

After multiplying both sides by e^{-st} dt and integrating from 0 to ∞, the following results

$$sY(x,s) - c_0 = D(\partial^2/\partial x^2)Y(x,s) \tag{C2}$$

which is rearranged to

$$(\partial^2/\partial x^2 - s/D)Y(x,s) = -c_0/D \tag{C3}$$

wherein

$$Y(x,s) \equiv \int_0^\infty dt e^{-st} c(x,t) \tag{C4}$$

is the Laplace transform of $c(x, t)$ and c_0 is the appropriate initial concentration.

In region A, $c_0 = c_A$ and the acceptable solution of eq C3 is

$$Y_A(x,s) = A\exp[-\sqrt{s/D}\,x] + c_A/s \tag{C5}$$

In region B, $c_0 = c_B$ and the solution of eq D3 is

$$Y_B(x,s) = B\exp[-\sqrt{s/D}\,x] + C\exp[\sqrt{s/D}\,x] + c_B/s \tag{C6}$$

The quantites A, B, and C are parameters to be determined.

The conditions imposed at the zone boundary are

$$c_A(x_0,t) = c_B(x_0,t) \tag{C7}$$

$$\partial c_A(x_0,t)/\partial x = \partial c_B(x_0,t)/\partial x \tag{C8}$$

which are Laplace transformed to

$$Y_A(x_0,s) = Y_B(x_0,s) \tag{C9}$$

$$\partial Y_A(x,s)/\partial x|_{x_0} = \partial Y_B(x,s)/\partial x|_{x_0} \tag{C10}$$

dx.doi.org/10.1021/jp302587d | J. Phys. Chem. B 2013, 117, 7626–7652

Condition C7 (continuous concentration) prevents infinite current density ($j = -D\partial c(x, t)/\partial x$) at x_0, and eq C8 (continuous current density) prevents an infinite accumulation (or loss) rate ($\partial c(x, t)/\partial t = D(\partial^2/\partial x^2)c(x, t)$) at $x = x_0$. Finally, the condition

$$\partial c_B(x, t)/\partial x|_{x=0} = 0 \tag{C11}$$

is imposed at $x = 0$. This zero current density condition is required to account for the obvious symmetry of the problem, which requires that $c(-x, t) = c(x, t)$ and, hence also $j(-x, t) = -j(x, t)$, and at the same time to prevent an infinite accumulation rate at $x = 0$. After Laplace transformation, eq C11 becomes

$$\partial Y_B(x, s)/\partial x|_{x=0} = 0 \tag{C12}$$

The three conditions C9, C10, and C12 suffice to determine the constants

$$A = (1/2)(c_B - c_A)(e^{\sqrt{s/D}\,x_0} - e^{-\sqrt{s/D}\,x_0})/s \tag{C13}$$

and

$$B = C = -(1/2)(c_B - c_A)\exp[-\sqrt{s/D}\,x_0]/s \tag{C14}$$

The following results finally

$$Y_A(x, s) = (1/2)(c_B - c_A)(1/s)(\exp[-\sqrt{s/D}\,(x - x_0)] - \exp[-\sqrt{s/D}\,(x + x_0)]) + c_A/s \tag{C15}$$

$$Y_B(x, s) = (-1/2)(c_B - c_A)(1/s)(\exp[-\sqrt{s/D}\,(x_0 - x)] + \exp[-\sqrt{s/D}\,(x_0 + x)]) + c_B/s \tag{C16}$$

The inverse Laplace transforms are found in standard tables to give finally

$$c_A(x, t) = ((c_B - c_A)/2)(\mathrm{erfc}[(x - x_0)/\sqrt{4Dt}\,] - \mathrm{erfc}[(x + x_0)/\sqrt{4Dt}\,]) + c_A \tag{C17}$$

$$c_B(x, t) = -((c_B - c_A)/2)(\mathrm{erfc}[(x + x_0)/\sqrt{4Dt}\,] + \mathrm{erfc}[(x - x_0)/\sqrt{4Dt}\,]) + c_B \tag{C18}$$

where erfc[x] is the complement of the error function. The quantity erfc[x] = 1 − erf[x] is evaluated in standard tables for values of the argument (x) from 0 to 3.5, at which point erfc[x] differs from 0 by less than 1 part in 10^5.

APPENDIX D. CROSS-DIFFUSION COEFFICIENT OF BSA AT PH 2.2

At pH 2.2, the carboxyl groups of BSA are not significantly ionized and its net charge, +92, is almost entirely due to protons bound to lysine, arginine, histidine, and α-amino groups. Leaist and Hao[38] studied cross-diffusion of dilute (10^{-4} M) BSA (component 3) in a two-component buffer consisting of 0.1 M H_3PO_4 (component 1) and 0.1 M KH_2PO_4 (component 2) at 25 °C. The hydrogen ion concentration, $c_{H^+} = 0.0065$ (pH 2.18), is reckoned by using the equilibrium constant, $K_d = 0.0076$, for the first dissociation reaction, $H_3PO_4 \rightleftharpoons H_2PO_4^- + H^+$, and ignoring the subsequent dissociations. According to classical multicomponent diffusion theory, the total BSA velocity in prevailing gradients of components 1 and 2 in the x-direction is

$$u = -(D_{31}/c_{BSA})\partial c_1/\partial x - (D_{32}/c_{BSA})\partial c_2/\partial x \tag{D1}$$

where D_{31} and D_{32} are the phenomenological cross-diffusion coefficients of BSA with components 1 and 2. Values measured by Leaist and Hao[38] were $D_{31} = (-1.3 \pm 0.5) \times 10^{-9}$ and $D_{32} = (+4.0 \pm 2.0) \times 10^{-10}$ cm^2/s. These values were compared with theoretical predictions, $D_{31} = -7.2 \times 10^{-9}$ and $D_{32} = -1.1 \times 10^{-8}$ cm^2/s, obtained from classical small-ion diffusion theory, which evidently greatly overestimates both magnitudes, and yields the wrong sign for D_{32}. The measured D_{31} and D_{32} should also provide useful tests of the present theory of chemotaxis.

First, we note that the concentration of component 2 is $c_2 = c_{K^+} = c_{salt}$ and that of component 1 is $c_1 = c_{H_3PO_4} + c_{H_2PO_4^-} - c_{K^+} = c_{H_3PO_4} + c_{H^+}$, after applying the electroneutrality condition, $c_{H_2PO_4^-} = c_{H^+} + c_{K^+} = c_{H^+} + c_{salt}$. Use of the equilibrium constant relation, $c_{H_3PO_4} = c_{H^+}c_{H_2PO_4^-}/K_d$, yields finally $c_1 = c_{H^+}(1 + (c_{H^+} + c_{salt})/K_d)$. After computing $\partial c_2/\partial x$ and $\partial c_1/\partial x$ from these expressions for c_1 and c_2 and inserting those into eq D1, the following results:

$$u = -(D_{31}/c_{BSA})(1 + (2c_{H^+} + c_{salt})/K_d)(c_{H^+})(\partial \ln c_{H^+}/\partial x) - [(D_{31}/c_{BSA})(c_{H^+}/K_d) + (D_{32}/c_{BSA})](c_{salt})(\partial \ln c_{salt}/\partial x) \tag{D2}$$

When proton binding to neutral basic groups predominates, as is the case for BSA at pH 2.2, the gradient factor in eqs 51, 59, and 60 becomes

$$G = (\partial \ln c_{H^+}/\partial x)_{T,P,c_P^\infty,c_{salt}} + W(\partial \ln c_S/\partial x)_{T,P,c_P^\infty,\hat{c}_{H^+}} = \left(1 + \left(\frac{c_{H^+}}{c_{H^+} + c_{salt}}\right)W\right)\left(\frac{\partial \ln c_{H^+}}{\partial x}\right) + \left(\frac{c_{salt}}{c_{H^+} + c_{salt}}\right)W\left(\frac{\partial \ln c_{salt}}{\partial x}\right) \tag{D3}$$

where the subscripts on the slopes have been suppressed in the last line. Inserting eq D3 into eq 59 yields

$$u = \frac{2kT\lambda}{3\eta A_1}\left\{\left(1 + \left(\frac{c_{H^+}}{c_{H^+} + c_{salt}}\right)W\right)\frac{\partial \ln c_{H^+}}{\partial x} + \left(\frac{c_{salt}}{c_{H^+} + c_{salt}}\right)W\frac{\partial \ln c_{salt}}{\partial x}\right\} \tag{D4}$$

Equating the coefficients of $\partial \ln c_{H^+}/\partial x$ and $\partial \ln c_{salt}/\partial x$ in eqs D2 and D4 yields two equations that can be solved to give

$$D_{31} = -c_{BSA}\left(\frac{2kT\lambda}{3\eta A_1}\right)\left(1 + \left(\frac{c_{H^+}}{c_{H^+} + c_{salt}}\right)W\right)\left(\frac{K_d}{c_{H^+}}\right)\frac{1}{(K_d + 2c_{H^+} + c_{salt})} \tag{D5}$$

$$D_{32} = -c_{BSA}\left(\frac{2kT\lambda}{3\eta A_1}\right)\left[\left(\frac{W}{c_{H^+} + c_{salt}}\right) - \left(1 + \left(\frac{c_{H^+}}{c_{H^+} + c_{salt}}\right)W\right)\frac{1}{(K_d + 2c_{H^+} + c_{salt})}\right] \tag{D6}$$

The ratio

dx.doi.org/10.1021/jp302587d | J. Phys. Chem. B 2013, 117, 7626−7652

$$D_{32}/D_{31}= \frac{\left[\left(\frac{W}{c_{H^+}+c_{salt}}\right)-\left(1+\left(\frac{c_{H^+}}{c_{H^+}+c_{salt}}\right)W\right)\frac{1}{(K_d+2c_{H^+}+c_{salt})}\right]}{\left(1+\left(\frac{c_{H^+}}{c_{H^+}+c_{salt}}\right)W\right)\left(\frac{K_d}{c_{H^+}}\right)\frac{1}{(K_d+2c_{H^+}+c_{salt})}} \quad \text{(D7)}$$

is independent of λ and A_{ch}. The theoretical result in eq D7 is equated to the ratio of measured values, $D_{32}/D_{31} = -0.31 \pm 0.19$, to evaluate $W = 0.59(+0.21, -0.20)$, where the negative deviation is associated with $D_{32}/D_{31} = -0.31 - 0.19 = -0.50$, and the positive deviation is associated with $D_{32}/D_{31} = -0.31 + 0.19 = -0.12$. Thus, W must lie in the range $0.39 \le W \le 0.80$, in order to fit the theory to the data. This in turn requires values of the electrostatic PIC per charge group in the range $-0.40 \le \Gamma_{1S}(P(NH^+)_N) \le -0.30$, and a similar range for $\partial\Gamma_S((P_{NH^+})_N)/\partial N$, where $P(NH^+)_N$ denotes the BSA with $N = 92$ bound protons. In order to judge whether this range is reasonable, it is helpful to know the area per H^+-binding group, A_{ch}, of an effective sphere model of BSA. The radius of the effective sphere is reckoned from the reported diffusion coefficient, $D_{33} = 7.0 \times 10^{-7}$ cm^2/s, of BSA under the prevailing conditions.[38] By using $R = kT/6\pi\eta D_{33} = 3.5 \times 10^{-7}$ cm, we obtain $A_{ch} = 4\pi R^2/92 = 167 \times 10^{-16}$ cm^2. The average distance between charges, $d = 2(A_{ch}/\pi)^{1/2} = 14.7 \times 10^{-8}$ cm, exceeds by 1.53-fold the Debye length, $1/\kappa = 9.6 \times 10^{-8}$ cm, under the prevailing 0.1 M ionic strength conditions. Thus, $\Gamma_{1S}(P(NH^+)_N)$ should lie significantly closer to its lower limit of −0.5 than to its upper (NLPB) limit of 0.0. Thus, the range (−0.40 to −0.30) of allowed values for $\Gamma_{1S}(P(NH^+)_N)$, and also for $\partial\Gamma_S((P_{NH^+})_N)/\partial N$, and their associated range of (0.39 to 0.80) of W, which is needed to fit the chemotactic theory to the measured D_{32}/D_{31} ratio, seem to be quite reasonable.

Given $A_{ch} \simeq 1.67 \times 10^{-16}$ cm^2 and $W = 0.59$ (+0.21, −0.20), the value of the slip length required to yield the measured values of D_{31} and D_{32} is $\lambda = 0.72 \pm 0.28$ Å. This value is roughly comparable to that ($\lambda = 0.47$ Å) estimated for carboxylated microspheres, when the W term is taken into account, as discussed in the main text.

APPENDIX E. ESTIMATION OF THE VELOCITY PROFILE

We consider a straight horizontal channel, open at the top, with a length much greater than its width, which in turn is somewhat greater than its depth. This channel is filled to a depth $z_0 = 3$ mm with an aqueous solution bearing uniform gradients, $d \ln c_{NaOH}/dx$ and $d \ln c_S/dx$, along the channel axis (x). The bottom surface of the channel is glass, which contains Γ silanol groups per unit area, some of which bind NaOH to provide a negative surface charge (due to SiO^- groups) plus Na^+ counterions. For simplicity, the sidewalls are assumed to be devoid of charges or groups that bind NaOH or HCl, and are assumed to exhibit slip boundary conditions so that the (assumed) uniform fluid velocity along the channel, $v_x(z)$, is independent of the horizontal y-coordinate perpendicular to the channel axis, and depends only upon the vertical distance z above the bottom. Taking the sidewalls into account with a no slip or partial slip boundary condition would yield somewhat smaller fluid velocities than those reckoned here even at the channel center. Also, for simplicity, we consider the limit of slow uniform fluid flow in a quasi-steady state, which could prevail only at relatively early times before the gradient of ln c_{NaOH} is so perturbed that it is substantially non-uniform.

The relevant Navier–Stokes equation for such a slow uniform flow is

$$\eta\frac{\partial^2 v_x(z)}{\partial z^2} = -F_b(z) \quad \text{(E1)}$$

where $F_b(z)$ is the force per unit volume (body force) exerted on the fluid by the glass bottom and η is the solution viscosity, which is taken to be a constant equal to that of water, which is an excellent approximation for the NaOH concentrations ($c_{NaOH} \le 10^{-3}$ M) considered here.

We consider an infinitesimal patch of glass surface with area $\delta A = dx\,dy$. The total force exerted on this patch by its adjacent fluid is

$$F^{pat} = \delta A k T f \Gamma G \quad \text{(E2)}$$

where Γ is the total number of OH^- binding sites per unit area and G is the gradient factor in eq 51. The total force exerted on the solution by the patch, F^{sol}, must be equal and opposite in sign to F^{pat}, hence $F^{sol} = -F^{pat}$. Although we do not know precisely how F^{sol} is distributed over the z-dimension in the solution, we do know that $\int_0^{z_0} F_b(z)\delta A\,dz = F^{sol}$, or equivalently that

$$\int_0^{z_0} F_b(z)\,dz = \frac{F^{sol}}{\delta A} = -kTf\Gamma G \quad \text{(E3)}$$

In general, one can write

$$F_b(z) = (F^{sol}/\delta A)p(z) = -kTf\Gamma G p(z) \quad \text{(E4)}$$

where $p(z)$ is a normalized distribution function such that $\int_0^{z_0} p(z)\,dz = 1.0$. The value $z = 0$ is taken at the surface, so $p(z)$ admits a finite range of surface–solution interaction. For simplicity, we choose

$$p(z) = (h/(1 - e^{-hz_0}))e^{-hz} \quad \text{(E5)}$$

which simply provides an integrable normalized distribution function with a mean width, $\langle z\rangle = 1/h$, when z_0 is sufficiently large that $hz_0 \gg 1.0$, as it is here.

After substituting eqs E4 and E5 into eq E1, both sides of E1 can be integrated from $z = z_0$ to z. Use of the boundary condition $\partial v_x(z_0)/\partial z = 0$ (no shear at the top surface) yields

$$\partial v_x z/\partial z = -(kTf\Gamma G/\eta)(e^{-hz} - e^{-hz_0})/(1 - e^{-hz_0}) \quad \text{(E6)}$$

At $z = 0$, this gives

$$\eta dv_x(0)/\partial z = -kTf\Gamma G \quad \text{(E7)}$$

which is the expected traction balance condition at the solution–glass boundary.

A further integration of eq E6 from $z = 0$ to z yields

$$v_x(z) = -(kTf\Gamma G/\eta)(1 - e^{-hz_0})^{-1}((1/h)(1 - e^{-hz}) - ze^{-hz_0}) + v_x(0) \quad \text{(E8)}$$

We consider two possible choices of $v_x(0)$.

(1) The traditional no slip boundary condition, $v_x(0) = 0$, yields

$$v_x(z) = -(kTf\Gamma G/\eta)(1 - e^{-hz_0})^{-1}(1/h)(1 - e^{-hz} - hze^{-hz_0}) \quad \text{(E9)}$$

dx.doi.org/10.1021/jp302587d | J. Phys. Chem. B 2013, 117, 7626–7652

If $hz_0 \gg 1.0$, then

$$v_x(z_0) = -(kTf\Gamma G/\eta)(1/h)(1 - e^{-hz}) \quad \text{(E10)}$$

If the range of the solution−surface interaction is $1/h = 10^{-9}$ cm, as expected for OH^--binding interactions, then $h = 10^9$ cm^{-1}. This would give $hz_0 = 3 \times 10^8$ for a 3 mm deep channel, so indeed $hz_0 \gg 1.0$. Although non-vanishing for $z \gg 1/h$, the predicted velocities for this no slip condition are rather small, as will be seen.

(2) The partial slip boundary condition, $v_x(0) = \lambda \partial v_x(0)/\partial z$, where λ is the slip length, yields

$$v_x(z) = -(kTf\Gamma G/\eta)(1 - e^{-hz_0})^{-1}h^{-1}\{1 - e^{-hz} - hze^{-hz_0} + h\lambda(1 - e^{-hz_0})\} \quad \text{(E11)}$$

In the limit $hz_0 \gg 1.0$, the predicted velocity is

$$v_x(z) \cong -(kTf\Gamma G/\eta)\{(1/h)(1 - e^{-hz}) + \lambda\} \quad \text{(E12)}$$

Whenever $hz_0 \gg 1.0$ and $\lambda \gg 1/h$, which is the case here, the fluid velocity profile corresponds to plug flow, except for a narrow zone of thickness, $1/h$, above the bottom surface.

Relevant slip lengths are $\lambda = 26-57$ nm for polished glass[61] and $\lambda \leq 1.0$ nm for plain pyrex and other possibly unpolished glass.[62]

In order to evaluate v_x, the surface density of ionized SiO^- groups, namely, Γf, is estimated following the protocol of Behrens and Grier.[59] The surface is assumed to exhibit $\Gamma = 8 \times 10^{18}$ potentially ionizable groups per m^2, typical of non-porous fully hydrated silica. The equilibrium constant expression for the proton dissociation reaction, $SiOH \rightleftharpoons SiO^- + H^+$, is

$$\frac{[H^+]_S\Gamma_{SiO^-}}{\Gamma_{SiOH}} = K_d \quad \text{(E13)}$$

where $[H^+]_S$ is the proton concentration near the surface and $K_d \simeq 10^{-7.5}$. The proton concentration near the surface is related to that ($[H^+]_B$) in the bulk solution far from the surface by

$$[H^+]_S = [H^+]_B e^{-e_0\psi_0/k_BT} \quad \text{(E14)}$$

where ψ_0 is the electrostatic potential at the surface and $e_0 = |e_0|$ is the protonic charge. The diffuse ion atmosphere is assumed to be separated from the surface by a thin counterion-free Stern layer across which the potential drops linearly from ψ_0 to ψ_d. The estimated phenomenological capacitance is $C = \sigma_{ch}/(\psi_0 - \psi_d) = 2.9$ F/m^2, where $\sigma_{ch} \equiv -e_0\Gamma_{SiO^-}$ is the average surface charge density. By combining the conservation equation, $\Gamma = \Gamma_{SiOH} + \Gamma_{SiO^-}$, with the above expressions for C and σ_{ch} and eqs E13 and E14, one can obtain

$$\psi_d(\sigma_{ch}) = (k_BT/e_0)\ln[-\sigma_{ch}/(e_0\Gamma + \sigma_{ch})] - (pH - pK_d)\ln[10](k_BT/e_0) - \sigma_{ch}/C \quad \text{(E15)}$$

Non-linear Poisson−Boltzmann theory yields

$$\sigma_{ch}(\psi_d) = 2\varepsilon\varepsilon_0\kappa(k_BT/e_0)\sinh[e_0\psi_d/2k_BT] \quad \text{(E16)}$$

where n is the total concentration of monovalent small ions, which are the only kind present, $\varepsilon_0 = 8.85 \times 10^{-12}$ F/m^2 is the dielectric susceptibility of free space, and $\kappa^2 \equiv e_0^2 n/(\varepsilon\varepsilon_0 k_BT)$. Equations E15 and E16 are readily solved for σ_{ch} and ψ_d by iteration for any choice of parameters. Then, $\Gamma f = \Gamma(\Gamma_{SiO^-}/\Gamma) = -\sigma_{ch}/e_0$ is the desired density of surface sites with bound OH^-. Calculations were performed for two conditions of interest. (1) For pH 10.0 NaOH, $n = (2 \times 10^{-4})(6.022 \times 10^{23})(1000) = 1.20 \times 10^{23}$ m^{-3}, and $\varepsilon = 80$, the following results: $\kappa = 3.27 \times 10^7$ m^{-1}, $\psi_d = -0.217$ V, $\sigma_{ch} = -0.0423$ C/m^2, $\Gamma f = 2.64 \times 10^{17}$ charges/m^2 $= 2.64 \times 10^{13}$ charges/cm^2, and $f = 0.033$. (2) For pH 9.0 NaOH, $n = (2 \times 10^{-5})(6.022 \times 10^{23})(1000) = 1.29 \times 10^{22}$ m^{-3}, and $\varepsilon = 80$, the following results: $\kappa = 1.037 \times 10^7$ m^{-1}, $\psi_d = -0.2046$ V, $\sigma_{ch} = -0.01063$ C/m^2, $\Gamma f = 6.64 \times 10^{16}$ charges/m^2 $= 6.64 \times 10^{12}$ charges/cm^2, and $f = 0.0083$.

For a channel with a uniform gradient, $d \ln c_{NaOH}/dx = -18.4$ cm^{-1}, corresponding to a decrease in c_{NaOH} from 10^{-3} to 10^{-7} M over a distance of 0.5 cm, the force exerted on the solution per unit area of glass surface at the point in the channel, where the pH is 10, is reckoned via eq E2 (with $W = 0$) to be $F^{sol}/\delta A = -F^{pat}/\delta A = -19.7$ dyn cm^{-2}. The predicted velocity of the fluid with the no slip boundary condition, when $1/h = 10^{-9}$ cm, at any $z \gg 1/h$ is predicted to be $v_x(z) = -1.97 \times 10^{-6}$ cm/s. The corresponding velocity of the fluid with the partial slip boundary condition at any $z \gg 1/h$ is found to be $v_x(z) = -1.97 \times 10^{-4}$ cm/s for $\lambda = 1.0$ nm, $v_x(z) = -5.1 \times 10^{-3}$ cm/s for $\lambda = 26$ nm, and $v_x(z) = -0.0112$ cm/s for $\lambda = 57$ nm.

At a point in the channel where $c_{NaOH} = 10^{-5}$ M, the calculated force on the solution per unit area of glass surface is $F^{sol}/\delta A = -4.94$ dyn/cm^2. In the no slip case with $1/h = 10^{-9}$ cm, the predicted velocity at any $z \gg 1/h$ is $v_x(z) = -4.94 \times 10^{-7}$ cm/s. In the partial slip case, the corresponding velocity at any $z \gg 1/h$ is $v_x(z) = -4.94 \times 10^{-5}$ cm/s for $\lambda = 1$ nm; $v_x(z) = -1.28 \times 10^{-3}$ cm/s for $\lambda = 26$ nm; and $v_x(z) = -2.82 \times 10^{-3}$cm/s for $\lambda = 57$ nm. The predicted velocities in the no slip case are so small that their measurement could be challenging, but in these relatively high pH regions of the gradient, significant fluid velocities are predicted for partial slip, whenever $\lambda \geq 1$ nm.

The predicted velocities differ substantially at different x-positions in the channel, because the fraction f of silanol groups that are ionized by OH^- binding declines with decreasing OH^- concentration. The different forces and induced velocities at different positions in the gradient will result in fluid pile-up and increasing fluid depth with decreasing x. Although these predicted velocities apply only to a transient state, they nevertheless provide useful approximate estimates, and illustrate the importance of the slip length as an essential determinant of the induced fluid velocity.

■ ASSOCIATED CONTENT

Supporting Information

Cross-diffusion theories for ionic solutions, theories of diffusiophoresis, thermodynamic analysis of neutral cosolute binding, approximate evaluation of Γ_{1S}, and thermodynamic analysis of the dissociation of the macromolecular acid groups in the presence of $H^+ + Cl^-$. This material is available free of charge via the Internet at http://pubs.acs.org.

■ AUTHOR INFORMATION

Corresponding Author

*Phone: 206-543-6681. Fax: 206-685-8665. E-mail: schurr@chem.washington.edu.

Notes

The authors declare no competing financial interest.

■ REFERENCES

(1) Onsager, L.; Fuoss, R. M. Irreversible Processes in Electrolytes Diffusion, Conductance, and Viscous Flow in Arbitrary Mixtures of Strong Electrolytes. *J. Phys. Chem.* **1932**, *36*, 2689−2778.

(2) Baldwin, R. L.; Dunlop, P. J.; Gosting, L. J. Interacting Flows in Liquid Diffusion. Equations for Evaluation of the Diffusion Coefficients from Moments of the Refractive Index Gradient Curves. *J. Am. Chem. Soc.* **1955**, *77*, 5235−5238.
(3) Dunlop, P. J.; Gosting, L. J. Interacting Flows in Liquid Diffusion. Expressions for the Solute Concentration Curves in Free Diffusion, and Their Use in Interpreting Gouy Diffusiometer Data for Aqueous 3-Component Systems. *J. Am. Chem. Soc.* **1955**, *77*, 5238−5249.
(4) Vanag, V. K.; Epstein, I. R. Cross-Diffusion and Pattern Formation in Reaction-Diffusion Systems. *Phys. Chem. Chem. Phys.* **2009**, *11*, 897−912.
(5) MacEwan, K.; Leaist, D. G. Quaternary Mutual Diffusion Coefficients for Aqueous Solutions of a Cationic-Anionic Mixed Surfactant from Moments Analysis of Taylor Dispersion Profiles. *Phys. Chem. Chem. Phys.* **2003**, *5*, 3951−3958.
(6) Vanag, V. K.; Rossi, F.; Cherkashin, A.; Epstein, I. R. Cross-Diffusion in a Water-in-Oil Microemulsion Loaded with Malonic Acid or Ferroin. Taylor Dispersion Method for Four-Component Systems. *J. Phys. Chem. B* **2008**, *112*, 9058−9070.
(7) Schurr, J. M.; Fujimoto, B. S. A Contribution to the Theory of Preferential Interaction Coefficients. *Biophys. J.* **2005**, *89*, 2258−2276.
(8) Leaist, D. G.; Lyons, P. A. Multicomponent Diffusion in Dilute-Solutions of Mixed Electrolytes. *Aust. J. Chem.* **1980**, *33*, 1869−1887.
(9) Leaist, D. G.; Lyons, P. A. Electrolyte Diffusion in Multi-component Solutions. *J. Phys. Chem.* **1982**, *86*, 564−571.
(10) Rard, J. A.; Miller, D. G. Ternary Mutual Diffusion-Coefficients of NaCl-$SrCl_2$-H_2O at 25 °C 0.1. Total Concentrations of 0.5 and 1.0 Mole dm^{-3}. *J. Phys. Chem. B* **1987**, *91*, 4614−4620.
(11) Leaist, D. G.; Al-Dahler, F. F. Predicting the Diffusion Coefficients of Concentrated Mixed Electrolyte Solutions from Binary Solution Data. NaCl+$MgCl_2$+H_2O and NaCl+$SrCl_2$+H_2O at 25 °C. *J. Chem. Eng. Data* **2000**, *45*, 308−314.
(12) Jakupi, P.; Halvorsen, H.; Leaist, D. G. A Thermodynamic Interpretation of the "Excluded-Volume Effect" in Coupled Diffusion. *J. Phys. Chem. B* **2004**, *108*, 7978−7985.
(13) Derjaguin, B. V.; Dukhin, S. S; Keptelova, M. M. Capillary Osmosis through Porous Partitions and Properties of Boundary-Layers of Solutions. *J. Colloid Interface Sci.* **1972**, *38*, 584−595.
(14) Dukhin, S. S.; Derjaguin, B. V. Electrokinetic Phenomena. In *Surface and Colloid Science*; Matijevic, E., Ed; Wiley: New York, 1974; Vol. *7*, Chapter 2.
(15) Anderson, J. L.; Prieve, D. C. Diffusiophoresis Caused by Gradients of Strongly Adsorbing Solutes. *Langmuir* **1991**, *7*, 403−406.
(16) Prieve, D. C.; Anderson, J. L.; Ebel, J. P.; Lowell, M. E. Motion of a Particle Generated by Chemical Gradients. 2. Electrolytes. *J. Fluid Mech.* **1984**, *148*, 247−269.
(17) Prieve, D. C.; Roman, R. Diffusiophoresis of a Rigid Sphere through a Viscous Electrolyte Solution. *J. Chem. Soc., Faraday Trans.* **1987**, *83*, 1287−1306.
(18) Ebel, J. P.; Anderson, J. L.; Prieve, D. C. Diffusiophoresis of Latex-Particles in Electrolyte Gradients. *Langmuir* **1988**, *4*, 396−406.
(19) Ajdari, A.; Bocquet, L. Giant Amplification of Interfacially Driven Transport by Hydrodynamic Slip: Diffusio-Osmosis and Beyond. *Phys. Rev. Lett.* **2006**, *96*, 186102−1- 186102−4.
(20) Anderson, J. L. Colloid Transport by Interfacial Forces. *Annu. Rev. Fluid Mech.* **1989**, *21*, 61−99.
(21) Munson, M. S.; Cabrera, C. R.; Yager, P. Passive Electrophoresis in Microchannels Using Liquid Junction Potentials. *Electrophoresis* **2002**, *23*, 2642−2652.
(22) Abècassis, B.; Cottin-Bizonne, C.; Ybert, C.; Ajdari, A.; Bocquet, L. Boosting Migration of Large Particles by Solute Contrasts. *Nat. Mater.* **2008**, *7*, 785−789.
(23) Zheng, J.-M.; Pollack, G. H. Long-Range Forces Extending from Polymer-Gel Surfaces. *Phys. Rev. E* **2003**, *68*, 031408-1−031408-7.
(24) Zheng, J.-M.; Chin, W. C.; Khijniak, E.; Khijniak, E., Jr.; Pollack, G. H. Surfaces and Interfacial Water: Evidence That Hydrophilic Surfaces Have Long-Range Impact. *Adv. Colloid Interface Sci.* **2006**, *127*, 19−27.
(25) Zheng, J.-M.; Pollack, G. H. Solute and Potential Distribution near Hydrophilic Surfaces. In *Water and the Cell*; Pollack, G. H., Cameron, I. L., Wheatley, D. N., Eds.; Springer: 2006; pp 165−174.
(26) Zhao, Q.; Zheng, J.-M.; Chai, B.; Pollack, G. H. Unexpected Effect of Light on Colloidal Crystal Spacing. *Langmuir* **2008**, *24*, 1750−1755.
(27) Zheng, J.-M.; Wexler, A.; Pollack, G. H. Effect of Buffers on Aqueous Solute-Exclusion Zones around Ion-Exchange Resins. *J. Colloid Interface Sci.* **2009**, *332*, 511−514.
(28) Nagornyak, E.; Yoo, H.; Pollack, G. H. Mechanism of Attraction between Like-Charged Particles in Aqueous Solution. *Soft Matter* **2009**, *5*, 3850−3857.
(29) Chai, B.; Yoo, H.; Pollack, G. H. Effect of Radiant Energy on Near-Surface Water. *J. Phys. Chem. B* **2009**, *113*, 13953−13958.
(30) Pollack, G. H.; Figueroa, X.; Zhao, Q. Molecules, Water, and Radiant Energy: New Clues for the Origin of Life. *Int. J. Mol. Sci.* **2009**, *10*, 1419−1429.
(31) Chai, B.; Pollack, G. H. Solute-Free Interfacial Zones in Polar Liquids. *J. Phys. Chem. B* **2010**, *114*, 5371−5375.
(32) Chai, B.; Zheng, J.-M.; Zhao, Q.; Pollack, G. H. Spectroscopic Studies of Solutes in Aqueous Solution. *J. Phys. Chem. A* **2008**, *112*, 2242−2247.
(33) Schurr, J. M.; McLaren, A. D. Kinetics of Trypsin Hydrolysis of Gelatin Spheres and Structure of Both Free-Solution and Gel-State Gelatin. *Enzymologia* **1965**, *29*, 315−368.
(34) Schurr, J. M.; McLaren, A. D. Enzyme Action. Comparison on Soluble and Insoluble Substrate. *Science* **1966**, *152*, 1064−1066.
(35) Schantz, E. J.; Lauffer, M. A. Diffusion Measurements in Agar Gel. *Biochemistry* **1962**, *1*, 658−663.
(36) Aragon, S.; Hahn, D. Precise Boundary Element Computation of Protein Transport Properties: Diffusion Tensors, Specific Volume, and Hydration. *Biophys. J.* **2006**, *91*, 1591−1603.
(37) Schurr, J. M. Phenomena Associated with Gel−Water Interfaces. Analyses and Alternatives to the Long-Range Ordered Water Hypothesis. *J. Phys. Chem. B* **2013**, DOI: 10.1021/jp302589y.
(38) Leaist, D. G.; Hao, L. Diffusion in Buffered Protein Solutions. Combined Nernst-Planck and Multicomponent Fick Equations. *J. Chem. Soc., Faraday Soc.* **1993**, *89*, 2775−2782.
(39) Schurr, J. M. Dynamic Light Scattering and Mutual Diffusion in Non-Ideal Systems. One-Component and Multicomponent Spherical Solutes. *Chem. Phys.* **1987**, *111*, 55−86.
(40) Allison, S. A.; Chang, E. L.; Schurr, J. M. Effects of Direct and Hydrodynamic Forces on Macromolecular Diffusion. *Chem. Phys.* **1979**, *38*, 29−41.
(41) Brenner, H. The Slow Motion of a Sphere through a Viscous Fluid towards a Plane Surface. *Chem. Eng. Sci.* **1961**, *16*, 242−251.
(42) Rushton, E.; Davies, G. Slow Unsteady Settling of Two Fluid Spheres along Their Line of Centers. *Appl. Sci. Res.* **1973**, *28*, 37−61.
(43) Batchelor, G. K. Sedimentation in a Dilute Dispersion of Spheres. *J. Fluid Mech.* **1972**, *52*, 245−268.
(44) Wolynes, P. G.; Deutch, J. M. Slip Boundary Conditions and Hydrodynamic Effect on Diffusion-Controlled Reactions. *J. Chem. Phys.* **1976**, *65*, 450−454.
(45) Honig, E. P.; Roeberson, G. J.; Wiersema, P. H. Effect of Hydrodynamic Interaction on Coagulation Rate of Hydrophobic Colloids. *J. Colloid Interface Sci.* **1971**, *36*, 97−109.
(46) Kirkwood, J. G.; Buff, F. P. The Statistical Mechanical Theory of Solutions.1. *J. Chem. Phys.* **1951**, *19*, 774−777.
(47) Ben-Naim, A. Solute and Solvent Effects on Chemical Equilibria. *J. Chem. Phys.* **1975**, *63*, 2064−2073.
(48) Ben-Naim, A. Theory of Preferential Solvation of Non-electrolytes. *Cell Biophys.* **1988**, *12*, 255−269.
(49) Ben-Naim, A. *Statistical Thermodynamics for Chemists and Biochemists*; Plenum Press: New York, 1992.
(50) Chitra, R.; Smith, P. E. Preferential Interactions of Cosolvents with Hydrophobic Solutes. *J. Phys. Chem. B* **2001**, *105*, 11513−11532.
(51) Smith, P. E. Cosolvent Interactions with Biomolecules: Relating Computer Simulation Data to Experimental Thermodynamic Data. *J. Phys. Chem. B* **2004**, *108*, 18716−18724.

(52) Smith, P. E. Equilibrium Dialysis Data and the Relationships between Preferential Interaction Parameters for Biological Systems in Terms of Kirkwood-Buff Integrals. *J. Phys. Chem. B* **2006**, *110*, 2862−2868.
(53) Smith, P. E. Chemical Potential Derivatives and Preferential Interaction Parameters in Biological Systems from Kirkwood-Buff Theory. *Biophys. J.* **2006**, *91*, 849−856.
(54) Batchelor, G. K. Brownian Diffusion of Particles with Hydrodynamic Interaction. *J. Fluid Mech.* **1976**, *74*, 1−29.
(55) Schurr, J. M. Polyanion Models of Nucleic Acid-Metal Ion Interactions. In *Nucleic Acid-Metal Interactions*; Hud, N. V., Ed.; RSC Publishing: Cambridge, U.K., 2009; Chapter 9, pp 308−349.
(56) Sharp, K. A.; Honig, B. Calculating Total Electrostatic Energies with the Nonlinear Poisson-Boltzmann Equation. *J. Phys. Chem. B* **1990**, *94*, 7684−7692.
(57) Sharp, K. A. Polyelectrolyte Electrostatics. Salt Dependence, Entropic, and Enthalpic Contributions to Free Energy in the Nonlinear Poisson-Boltzmann Model. *Biopolymers* **1995**, *36*, 227−244.
(58) Sharp, K. A.; Friedman, R.; Misra, V.; Hecht, J.; Honig, B. Salt Effects on Polyelectrolyte-Ligand Binding. Comparison of Poisson-Boltzmann and Limiting Law Counterion Binding Models. *Biopolymers* **1995**, *36*, 245−262.
(59) Behrens, S. V.; Grier, D. G. The Charge of Glass and Silica Surfaces. *J. Chem. Phys.* **2001**, *115*, 6716−6721.
(60) Maier, H. Electrorotation of Colloidal Particles and Cells Depends on Surface Charge. *Biophys. J.* **1977**, *73*, 1617−1626.
(61) Huang, P.; Guasto, J. S.; Breuer, K. S. Direct Measurement of Slip Velocities Using Three-Dimensional Total Internal Reflection Velocimetry. *J. Fluid Mech.* **2006**, *566*, 447−464.
(62) Bouziques, C. I.; Bocquet, L.; Charlais, E.; Cottin-Bizonne, C.; Cross, B.; July, L.; Steinberger, A.; Ybert, C.; Tabeling, P. Using Surface Force Apparatus, Diffusion and Velocimetry to Measure Slip Lengths. *Philos. Trans. R. Soc., A* **2008**, *366*, 1455−1468.
(63) Sha, Y.; Chen, H.; Yin, Y.; Tu, S.; Ye, L.; Zheng, Y. Characteristics of the Marangoni Convection Induced in Initial Quiescent Water. *Ind. Eng. Chem. Res.* **2010**, *49*, 8770−8777.
(64) Jungwirth, P.; Tobias, D. J. Specific Ion Effects at the Air/Water Interface. *Chem. Rev.* **2006**, *106*, 1259−1281.
(65) Darrington, I. M.; Butler, T. Z.; Collins, M. D.; Manrao, E.; Pavlenok, M.; Niederweis, M.; Gundlach, J. H. Nanopore DNA Sequencing with MspA. *Proc. Natl. Acad. Sci. U.S.A.* **2010**, *107*, 16060−16065.